Within-host evolution of SARS-CoV-2 in an immunosuppressed COVID-19 patient: a source of immune escape variants

Authors: Sebastian Weigang[1,7], Jonas Fuchs[1,7], Gert Zimmer[2], Daniel Schnepf[1], Lisa Kern[1], Julius Beer[1], Hendrik Luxenburger[3], Jakob Ankerhold[1], Valeria Falcone[1], Janine Kemming[3], Maike Hofmann[3], Robert Thimme[3], Christoph Neumann-Haefelin[3], Svenja Ulferts[4], Robert Grosse[4], Daniel Hornuss[5], Yakup Tanriver[6], Siegbert Rieg[5], Dirk Wagner[5], Daniela Huzly[1], Martin Schwemmle[1], Marcus Panning[1,8]*, Georg Kochs[1,8]*

[1]Institute of Virology, Freiburg University Medical Center, Faculty of Medicine, University of Freiburg, Freiburg, Germany

[2]Institute of Virology and Immunology, Mittelhaeusern, Switzerland

[3]Department of Medicine II, Freiburg University Medical Center, Faculty of Medicine, University of Freiburg, Freiburg, Germany

[4]Institute of Experimental and Clinical Pharmacology and Toxicology, Freiburg University Medical Center, Faculty of Medicine, University of Freiburg, Freiburg, Germany

[5]Division of Infectious Diseases, Dept. Med. II, Freiburg University Medical Center, Faculty of Medicine, University of Freiburg, Freiburg, Germany

[6]Division of Nephrology, Dept. Med. IV, Freiburg University Medical Center, Faculty of Medicine, University of Freiburg, Freiburg, Germany

[7]These authors contributed equally: Sebastian Weigang, Jonas Fuchs.

[8]These authors jointly supervised this work: Marcus Panning, Georg Kochs.

*correspondence to e-mail: georg.kochs@uniklinik-freiburg.de; marcus.panning@uniklinik-freiburg.de

Abstract

The recent emergence of SARS-CoV-2 variants showing increased transmissibility and immune escape is a matter of global concern. Their origin remains unclear, but intra-host virus evolution during persistent infections could be a contributing factor. Here, we studied the long-term SARS-CoV-2 infection in an immunosuppressed organ transplant recipient. Frequent respiratory specimens were tested for variant viral genomes by RT-qPCR, next-generation sequencing (NGS), and virus isolation. Late in infection, several virus variants emerged which escaped neutralization by COVID-19 convalescent and vaccine-induced antisera and had acquired genome mutations similar to those found in variants of concern first identified in UK, South Africa, and Brazil. Importantly, infection of susceptible hACE2-transgenic mice with one of the patient's escape variants elicited protective immunity against re-infection with either the parental virus, the escape variant or the South African variant of concern, demonstrating broad immune control. Upon lowering immunosuppressive treatment, the patient generated spike-specific neutralizing antibodies and resolved the infection. Our results indicate that immunocompromised patients are an alarming source of potentially harmful SARS-CoV-2 variants and open up new avenues for the updating of COVID-19 vaccines.

Key words: SARS-CoV-2, COVID-19, immunosuppression, transplant recipient, viral persistence and shedding, viral evolution, variants of concern, neutralizing antibodies,

Introduction

Individuals infected with SARS-CoV-2 develop neutralizing spike-specific antibodies that persist for months and protect against reinfection[1]. Similarly, neutralizing antibodies generated after vaccination efficiently protect from COVID-19[2]. However, the recent emergence of SARS-CoV-2 variants in the UK (B.1.1.7), South Africa (B.1.351) and Brazil (P.1)[3-5] pose a global threat due to their increased transmissibility and resistance to neutralizing antibodies[2]. The origin of these virus variants remains unclear, but long-term-infected immunocompromised individuals are a likely source, allowing prolonged viral replication and unhindered adaption to the host[6,7].

In Germany, the SARS-CoV-2 epidemic started with local outbreaks in February 2020. The city of Freiburg at the border to France and Switzerland was a hotspot due to multiple unrecognized infection events in March 2020. Therefore, immunocompromised patients were closely monitored, as these individuals were expected to have an increased risk of developing severe COVID-19 illness and to suffer from long-term persistent infection with prolonged viral shedding.

Here, we describe an immunosuppressed organ transplant recipient who acquired SARS-CoV-2 during the early phase of the COVID-19 pandemic. The patient had mild respiratory symptoms and was tested positive for SARS-CoV-2 for over 145 days. During this long period, virus variants with multiple amino acid substitutions and deletions in the spike protein evolved that showed increased resistance to neutralizing antibodies, suggesting partial immune escape. Interestingly, however, one of the late virus variants isolated from the patient elicited a broad protective immune response in experimentally infected mice, suggesting that convalescent individuals might become resistant against reinfection by emerging variants of concern.

Results

Clinical presentation of the organ transplant patient persistently infected with SARS-CoV-2.

A male person in his 50´s was admitted in spring 2020 to the University Medical Center, Freiburg, for transplantation. The patient was treated with a cocktail of tacrolimus, mycophenolate and prednisone for 7 month (Fig. 1a and b).

The patient was tested positive for SARS-CoV-2 by reverse transcription quantitative polymerase chain reaction (RT-qPCR) which is indicated with day 0(Fig. 1d). The source of infection remained unknown but strict infection prevention measures were initiated. No respiratory symptoms at the time of diagnosis were observed but a CT scan showed mild ground-glass opacities and discrete bilateral pleural effusions on day 4. The patient remained SARS-CoV-2 positive in the following weeks and was therefore kept in isolation. Two month after transplantation the patient suffered from a urinary tract infection with *E. coli*, requiring antibiotic treatment. Furthermore, he was treated for 5-days (day 56 to 60) with Ivermectin (33 mg/day) (Fig. 1c), a broad-spectrum drug with anti-viral activity in cell culture against several viruses including SARS-CoV-2[8,9]. While the bacterial urinary tract infection was controlled, the infection with SARS-CoV-2 was not.

RT-qPCR positive swab samples were used to successfully isolate virus on VeroE6 cells confirming shedding of infectious SARS-CoV-2 (Fig. 1e). Due to his critical condition, the patient stayed in the hospital until day 72 when he was discharged for home quarantine. However, he was re-hospitalized at day 106 to 126. Afterwards, the immunosuppressive regimen was modified by withdrawing mycophenolate mofetil treatment and by increasing the dose of prednisone (day 126) to allow for a better antiviral adaptive immune response. After re-admission at day 140 for control purposes, the patient was still RT-qPCR positive. As an attempt to control the infection, he was treated for 10 days with Remdesivir (200 mg on day 140, then 100 mg/daily, day 141 - 149), a nucleoside analog with anti-SARS-CoV-2 activity *in vitro*[10] and *in vivo*[7,11]. Subsequently, negative RT-qPCR tests until day 189 and failed virus isolation attempts suggested that the infection had resolved (Fig. 1d and e) (Extended Table 1).

Nucleoprotein (N)-specific antibodies were detected already 12 days after the first positive qPCR result and afterwards surged rapidly (Fig. 1f). In contrast, IgG antibody levels specific for SARS-CoV-2 spike

protein (S1) determined by ELISA constantly oscillated around the cutoff value between days 40 and 123. Only, when the patient was hospitalized at day 140, high levels of S1-specific IgG were detected and persisted at least until day 175 (Fig. 1f). Concomitantly with the increased spike-specific antibodies and the onset of Remdesivir treatment (day 140), RT-qPCR analysis showed steadily increasing Ct values, indicating diminishing virus replication (Fig. 1d and Extended Table 1). In summary, during the 25 weeks of infection with SARS-CoV-2 the patient had no severe respiratory or systemic symptoms and was finally able to clear the virus, likely due to the development of neutralizing antibodies and possibly due to the inclusion of antiviral Remdesivir treatment.

Genetic relationship of the patient´s SARS-CoV-2 variants with circulating strains. Full-length SARS-CoV-2 genome sequences were obtained from oropharyngeal swabs collected between day 0 and 140 and phylogenetic trees were constructed including sequences representative for the Freiburg area in spring 2020 (Fig. 2a) or a set of randomly selected GISAID sequences of isolates collected in Germany in spring 2020(Fig. 2b). The viral genomic sequences obtained from the patient clearly clustered to those of strains circulating in spring in Germany and in the Freiburg area (Fig. 2a and b). The phylogenetic analysis also demonstrated a close relationship with sequences obtained from two patients of the Medical Center Freiburg (Fig. 2a). However, no clear epidemiologic link was found between the immunosuppressed and the other two patients.

Analysis of the viral RNA that has been extracted from the patient samples revealed several nucleotide substitutions in ORF1ab, the spike gene, ORF3a, M and N genes in comparison to the Wuhan-Hu-1 reference genome (Fig. 2c). The continuous presence of nine common mutations in all sequences argues against a possible reinfection but is compatible with viral persistence. Within the first two weeks, no changes in the viral genome were observed, while from day 42 onward acquisition of several mutations occurred. Apart from low frequency mutations, some mutations accumulated over time indicative for the selection of distinct variants. The mutation 23403G resulting in the D614G substitution marks the genotype that now dominates worldwide[12].

The most remarkable changes found in the S gene, which were confirmed by Sanger sequencing of cDNA clones, were in-frame deletions and non-synonymous substitutions in the N-terminal domain (NTD) and the receptor binding motif (RBM) (Fig. 2d), respectively. Interestingly, the two amino acid

deletions in the NTD were associated with specific single amino acid substitutions in the RBM: del141-144 with F490L and del244-247 with E484G. Both deletions, which are located in two adjacent flexible loops of the NTD (Fig. 3), might affect the conformation of this subdomain and are targets of neutralizing antibodies[13,14]. The two amino acid substitutions (E484G and F490L) may lead to subtle conformational changes in the RBD, which is the main target of neutralizing antibodies and a known hotspot for mutations conferring escape from neutralizing antibodies[15-17]. Thus, the SARS-CoV-2 spike variants from the immunosuppressed patient share mutations with the escape variants of concern from the UK, South Africa and Brazil (Fig. 2e).

Prolonged viral persistence resulted in impaired viral fitness. In the early phase of viral persistence (days 0 to 34) virus isolation was successful, indicating constant virus shedding (Fig. 1e). We repeatedly failed, however, to isolate virus thereafter when the Ct values increased above 25. On day 105, the Ct value dropped to 23 and virus isolation was again successful (Fig. 1e). The sequences of the two distinct virus isolates obtained at day 14 (d14) and day 105 (d105) were compared to the corresponding sequences obtained from swab samples of the same day. While the sequences of the d14 isolate and the d14 swab were identical, the sequence of the d105 isolate partially differed from the d105 swab sequence (Fig. 4a). The viral genome sequences of the d105 isolate and the swab samples contained the amino acid deletion 244-247 combined with the E484G mutation, while the amino acid deletion del141-144 and the F490L substitution were only found in the swab samples. Since the majority of the mutations in the d105 isolate was also detected in the swab samples, the d105 virus might represent an abundant genotype that was selected during persistence in the patient. However, we cannot exclude that some alterations were introduced during the process of virus isolation in cell culture including a frame shift deletion in ORF7b and a deletion of 21 nucleotides (del23601-23621) in about 50% of the reads that mapped to the spike gene and resulted in the replacement of the eight amino acids SPRRARSV by a single leucine upstream of the S1/S2 cleavage site (Fig. 4a).

The d14 and d105 isolates both showed accumulation of viral N- and spike proteins in infected cells by indirect immunofluorescence and Western blot analyses (Fig. 4b and c). In VeroE6 cells, both isolates grew to comparable titers, whereas replication of the d105 isolate was impaired in human lung adenocarcinoma Calu-3 cells (Fig. 4d). To confirm the attenuated phenotype of d105 *in vivo*, K18-

hACE2 mice encoding the human SARS-CoV-2 receptor, angiotensin-converting enzyme type 2 (ACE2)[18] were intranasally infected with two different doses of the d14 and d105 isolates (200 or 2000 plaque-forming units (pfu)). Animals infected with the d14 isolate showed a significant weight loss within 4 to 8 days. One out of eight animals infected with 200 pfu survived the infection, whereas all animals infected with 2000 pfu had to be euthanized due to severe disease symptoms or weight loss (Fig. 4e and f). In contrast, K18-hACE2 mice infected with the d105 isolate showed a transient weight loss but only two out of seven animals infected with 2,000 pfu got severely sick and had to be sacrificed (Fig. 4e and f), highlighting the attenuated phenotype of this isolate. Together these findings suggest that the mutations in the viral genome of the d105 isolate caused reduced viral fitness.

SARS-CoV-2 escape variants emerged during viral persistence. The amino acid deletions and substitutions in the spike proteins of the emerging viral variants could have been selected by the antiviral immune response of the host. To address this issue, serum samples of the patient were tested for neutralizing antibodies in a plaque reduction assay performed with either the d14 or the d105 virus isolate. Only sera collected from the patient after day 123 showed SARS-CoV-2 neutralizing activity (Fig. 5a), which coincided with the increase of S-specific IgG between day 123 and 140 (Fig. 1f). Intriguingly, while the d14 isolate was efficiently neutralized up to serum dilutions of 1:128, the d105 virus was poorly inhibited even at the lowest serum dilutions used (1:32) (Fig. 5a), suggesting that the substitutions in the d105 spike protein caused escape from neutralizing antibodies. The neutralization titers detected in sera from the immunosuppressed patient were generally lower than those detected in serum from an immunocompetent convalescent COVID-19 patient (Fig. 5a, positive control). Similarly, antisera of convalescent COVID-19 patients and of individuals previously vaccinated with the BNT162b2 mRNA vaccine (Pfizer/BioNTech) showed higher neutralizing activity against the d14 isolate as compared to the d105 isolate (Fig. 5b).

To independently determine the neutralization titer 50 (NT_{50}) of convalescent sera against the various spike variants found in the patient, we made use of a virus pseudotype system based on single-cycle vesicular stomatitis virus (VSV) vector encoding a firefly luciferase reporter, VSV*ΔG(FLuc). High NT_{50} values were observed with the d14 spike protein (Fig. 5c). In contrast, pseudotype virus bearing

the d105 spike protein was neutralized with significantly lower efficacy as indicated by a 8.3-fold reduced NT_{50} value (Fig. 5c).

Next, we analyzed pseudotype virus harboring the d14 spike protein with single or combined mutations including del244-248 and E484G (for d105) and del141-144 and F490L (for d140) (Fig. 2d). Compared to pseudotype virus displaying the parental d14 spike protein, viruses pseudotyped with either the E484G or the F490L mutant spike proteins were equally well neutralized by a COVID-19 convalescent serum, whereas pseudotype virus bearing spike proteins with the amino acid deletions del141-144 or del244-247 were significantly less well neutralized (Fig. 5d). The combination of the amino acid deletions del141-144 or del244-247 with either E484G or F490L did not further reduce neutralization efficacy. A different pattern was observed when immune serum from a person who had been immunized with an mRNA-based SARS-CoV-2 vaccine was analyzed (Fig. 5e). Using this immune serum, virus pseudotyped with the E484G mutant spike was less well neutralized than virus bearing the parental spike protein. Furthermore, pseudotype virus displaying spike protein containing both the E484G substitution and the del141-144 deletion, was less efficiently neutralized than pseudotype viruses containing either E484G or del141-144, suggesting that the two mutations acted in a synergistic manner. In summary, the amino acid changes del141-144 and del244-247, both located in the NTD, and E484G in the RBD all affect crucial antigenic regions[19] which were selected during viral persistence as they allow escape of SARS-CoV-2 from the humoral immune response.

SARS-CoV-2 escape variant d105 induces broad protective immunity *in vivo*. The reduced neutralization capacity of the patient`s sera against the d105 isolate raised the question whether the changes in the spike protein might have compromised the induction of an efficient antiviral immune response. To address this question, sera from K18-hACE2 mice that survived the infection with the d14 or the d105 isolates (Fig. 4e and f) were collected 21 days post infection or later. We also prepared sera from K18-hACE2 mice surviving infection with the Muc-IMB-1 isolate, lineage B.1, encoding an identical spike protein sequence like the d14 isolate[20], in order to increase the number of convalescent sera of animals surviving infection with wild-type SARS-CoV-2. The sera of the animals that survived infection with the wild-type viruses had about 2-fold higher levels of SARS-CoV-2-specific IgG

antibodies (assessed by an immunofluorescence-based assay), than the sera of mice that survived the milder d105 infection (Fig. 6a).

The capacity of sera obtained from the d14- and Muc-IMB-1-infected mice to neutralize the d105 isolate was some 4-fold lower than the neutralizing capacity against the d14 isolate (Fig. 6b), indicating partial immune escape of the d105 isolate. Intriguingly, the d105 mouse sera neutralized the d105 virus more efficiently than the d14 isolate (Fig. 6c). Additionally, we tested the neutralization capacity of the convalescent mouse sera against two recent German isolates of the UK (B.1.1.7) and the South Africa (B.1.351) variants of concern. Sera of wild-type-infected mice were more effective in neutralizing the B.1.1.7 virus variant than the B.1.351 variant (Fig. 6d). However, the opposite was observed using sera from d105-infected animals since the B.1.351 variant demonstrated a higher sensitivity to neutralization by the d105 sera than the B.1.1.7 variant (Fig. 6e). Finally, all convalescent animals, including those infected with Muc-IMB-1, were challenged with a lethal dose (100,000 pfu) of either the d14 or the d105 virus isolate one to four months after the first infection. In contrast to the naïve control animals, all convalescent mice survived the challenge infection without any signs of disease or weight loss (Fig. 6f and g), demonstrating that the animals were protected against challenge infection by both virus variants.

SARS-CoV-2 specific CD8+ T cells are not driving emergence of escape variants. Finally, we assessed whether the variations in the spike S1 domain also resulted in an escape from the CD8+ T cell response. We performed *in silico* prediction of CD8+ T cell epitopes within the SARS-CoV-2 S1 domain restricted by the HLA class I alleles of the immunosuppressed COVID-19 patient (HLA-A*02:01, HLA-A*03:01, HLA-B*51:01, HLA-B*56:01). Using ANN4.0 of the Immune Epitope Database website[21] we identified one nonamer peptide within the NTD with good binding properties to HLA-A*02:01 ($S_{133-141}$ FQFCNDPFL) and another nonamer peptide ($S_{142-150}$ GVYYHKNNK) with binding to HLA-A*03:01, both overlapping with del141-144. In addition, we identified a decamer peptide ($S_{240-249}$) with potential binding to HLA-A*02:01 that overlaps with del244-247. Further CD8+ T cell epitope peptides overlapping with the E484G or F490L substitutions could not be predicted. Subsequently, we tested whether the selected peptides represent SARS-CoV-2-specific CD8+ T cell epitopes by incubating PBMCs from the convalescent, immunosuppressed COVID-19 patient on day 233 or from

immunocompetent, convalescent, HLA-A*02:01/HLA-A*03:01 positive COVID-19 patients with the peptides for 14 days. However, after stimulation with the selected peptides neither PBMCs from the immunosuppressed nor from the convalescent donors showed any IFNγ-positive CD8+ T cell response whereas a weak IFNγ-positive CD8+ T cell response targeting the non-overlapping epitope HLA-A*03:01/$S_{378-386}$ was detectable in PBMCs from the immunosuppressed patient (Extended Data Fig. 1). This observation indicates that the predicted SARS-CoV-2 peptides that overlap with the mutated S1 regions do not represent CD8+ T cell epitopes. Hence, the mutations within the S1 regions of the d105 and d140 spike proteins were most probably not selected due to CD8+ T cell escape, but to escape from the humoral response.

Discussion

Circulating SARS-CoV-2 variants typically acquire only few mutations over time which accumulate at a relatively constant rate of about 1-2 mutations per month[22]. Accordingly, the predominant virus genotypes initially found in swab samples during the first weeks of the persistent infection of the immunocompromised patient were relatively stable and grouped into Nextstrain clade 20B, Pangolin lineage B.1.1, together with simultaneously circulating variants (Fig. 2a and b). However, from day 42 onward, synonymous and non-synonymous mutations accumulated in the viral genomes, including two in-frame amino acid deletions in the NTD (del141-144 and del244-247) as well as two single amino acid exchanges (E484G and F490L) in the RBM. Interestingly, the substitutions in the RBM were exclusively associated with one or the other of the deletions, namely F490L with del141-144 and E484G with del244-247, respectively. This striking interlinked coevolution may have been favored by the necessity to preserve the functionality or stability of the spike protein and to maintain or improve viral fitness. The loops N3 (130-150) and N5 (240-260) that are affected by the two NTD deletions are a preferred target of in-frame deletions of variable length and are therefore referred to as “recurrent deletion regions”[14].

Of note, the transient and altering patterns of amino acid changes in the viral spike protein were most likely the result of an ongoing conflict between the persisting virus and the patient’s adaptive immune system. The rather weak spike-specific antibody response between days 40 to 123 presumably selected

for spike escape variants, as demonstrated by their reduced sensitivity to inhibition by immune sera obtained from the patient at later time points, or from convalescent COVID-19 patients, as well as from COVID-19 vaccinated individuals. It is conceivable that prolonged viral replication in immunosuppressed patients can lead to the emergence of new immune-escape variants, such as the SARS-CoV-2 variants of concern like UK B.1.1.7, South Africa B.1.351 and Brazil P.1. They all share mutations in the same regions of the spike protein as the escape variants described in this study (Fig. 2e). Accumulation of amino acid substitutions or deletions in similar regions of the spike protein were reported before for isolates of persistently infected, immunosuppressed patients[6,7] and also for isolates from patients treated with antibody cocktails and convalescent plasma[7,15,23].

The reasons for the late but sudden rise of spike-specific antibodies in the patient serum between day 123 and 141 are not clear. We suspect that the pausing of mycophenolate mofetil from day 126 until day 175 favored broad, spike-specific antibody response that finally terminated the infection. To allow spike-specific antibody production, discontinuation of mycophenolate mofetil treatment of COVID-19-infected transplant recipients is advisable and in line with current clinical guidelines e.g. of the British Transplantation Society (https://bts.org.uk/information-resources/covid-19-information/, updated 22nd January 2021). Adjusting immunosuppressive medications appears to be crucial for induction of an antiviral immune response and clearance of SARS-CoV-2[24].

Postinfection sera from mice that survived infection with wild-type virus demonstrated reduced neutralizing activity against the late d105 virus isolate, highlighting the antibody escape phenotype of this variant. Conversely, sera from mice previously infected with the d105 isolate more efficiently neutralized the d105 variant than the d14 virus. Hence, broadly neutralizing antibodies that were elicited by new immunogenic epitopes exposed on the mutated d105 spike protein may have controlled the escape variant in the persistently infected patient. To confirm such an extended neutralizing activity of the d105 immune sera, we used recent virus variants of concern and detected enhanced neutralization of the South Africa B.1.351 variant by the d105 antisera when compared to the UK B.1.1.7 variant. These findings match with recent analyses of convalescent plasma samples from patients that recovered from B.1.351 infections. Cele et al. showed efficient neutralization of an early 2020 isolate as well as of the late South African variant of concern by these convalescent antisera [25]. Because these globally emerging

viruses show a clear escape from vaccine induced humoral immunity[2,26,27], our findings might be important for the redesign of future vaccines.

The SARS-CoV-2 d105 variant that was isolated from the patient throat swab at a late stage of his disease showed reduced viral fitness in Calu-3 cell cultures and in K18-hACE2 mice, but not in VeroE6 cells. The reason for attenuation and the causative mutations in the viral genome are presently not known, but the observed viral growth restriction might depend on host cell-intrinsic innate restriction factors. In addition, we detected a 21 nucleotide-long deletion in the multi basic cleavage site of the spike protein connecting the S1 and S2 subdomains. Additional mutations included a truncation of ORF7b, encoding an accessory protein with yet unknown biological function. Deletions in ORF7b have been described in an early Asian cluster of SARS-CoV-2 without a sign of attenuation[28] as well as in a SARS-CoV/2003 clone[29]. As recently shown[30], we assume that the loss of the multibasic furin cleavage site during isolation in VeroE6 cells contributed to the attenuation of the d105 isolate.

In summary, we detected SARS-CoV-2 variants in a persistently infected immunocompromised patient which partially escaped the humoral immune response. Such escape mutants could serve as initial seed for newly emerging variants with enhanced epidemic potential, especially if they overcome impaired viral fitness by further adaptation. Unexpectedly, the spike protein of this escape variant worked particularly well in immunization approaches and elicited broadly active neutralizing antibodies able to control SARS-CoV-2 variants of concern.

Acknowledgements

This work was supported by the Bundesministerium fuer Bildung und Forschung (BMBF) through the Deutsches Zentrum fuer Luft- und Raumfahrt, Germany, (DLR, grant number 01KI2077) to MP, RT and MS and by the Federal State of Baden-Wuerttemberg, Germany, MWK-Sonderfoerdermaßnahme COVID-19/AZ.:33-7533.-6-21/7/2 to MS and AZ33-7533-6-10/89/8 to CNH. The funders had no role in the study design, data analysis, data interpretation, and in the writing of this report. All authors had full access to the data in the study and accept responsibility to submit for publication.

Author contributions

MH, GK, CNH, MP, DS, MS, SW and GZ designed the study and contributed to experimental design and data interpretation. DH, JK, HL, SR, YT and DW preformed patient recruitment, clinical management, evaluation of clinical data and sample collection. JF and LK performed bioinformatic analyses. JA, JB, JF, VF, RG, DH, JK, HL, DS, SU, SW and GZ performed experiments and analyzed and processed the data. JF, MH, GK, MP, MS and GZ wrote the manuscript. MH, GK, CNH, MP, MS and RT were involved in funding acquisition.

Competing interests

All authors declare to have no financial or other associations that might pose a potential or actual conflict of interest.

References (60)

1. Wajnberg, A., *et al.* Robust neutralizing antibodies to SARS-CoV-2 infection persist for months. *Science* **370**, 1227-1230 (2020).
2. Wang, Z., *et al.* mRNA vaccine-elicited antibodies to SARS-CoV-2 and circulating variants. *Nature* (2021).
3. Rambaut, A. & Loman, N. Preliminary genomic characterisation of an emergent SARS-CoV-2 lineage in the UK defined by a novel set of spike mutations. *ARTIC Network* (2020).
4. Tegally, H., *et al.* Sixteen novel lineages of SARS-CoV-2 in South Africa. *Nat Med* (2021).
5. Candido, D.S., *et al.* Evolution and epidemic spread of SARS-CoV-2 in Brazil. *Science* **369**, 1255-1260 (2020).
6. Avanzato, V.A., *et al.* Case Study: Prolonged Infectious SARS-CoV-2 Shedding from an Asymptomatic Immunocompromised Individual with Cancer. *Cell* **183**, 1901-1912 e1909 (2020).
7. Choi, B., *et al.* Persistence and Evolution of SARS-CoV-2 in an Immunocompromised Host. *N Engl J Med* **383**, 2291-2293 (2020).
8. Caly, L., Druce, J.D., Catton, M.G., Jans, D.A. & Wagstaff, K.M. The FDA-approved drug ivermectin inhibits the replication of SARS-CoV-2 in vitro. *Antiviral Res* **178**, 104787 (2020).
9. Lehrer, S. & Rheinstein, P.H. Ivermectin Docks to the SARS-CoV-2 Spike Receptor-binding Domain Attached to ACE2. *In Vivo* **34**, 3023-3026 (2020).
10. Gordon, C.J., *et al.* Remdesivir is a direct-acting antiviral that inhibits RNA-dependent RNA polymerase from severe acute respiratory syndrome coronavirus 2 with high potency. *J Biol Chem* **295**, 6785-6797 (2020).
11. Buckland, M.S., *et al.* Treatment of COVID-19 with remdesivir in the absence of humoral immunity: a case report. *Nat Commun* **11**, 6385 (2020).
12. Korber, B., *et al.* Tracking Changes in SARS-CoV-2 Spike: Evidence that D614G Increases Infectivity of the COVID-19 Virus. *Cell* **182**, 812-827 e819 (2020).
13. Walls, A.C., *et al.* Structure, Function, and Antigenicity of the SARS-CoV-2 Spike Glycoprotein. *Cell* **183**, 1735 (2020).
14. McCarthy, K.R., *et al.* Recurrent deletions in the SARS-CoV-2 spike glycoprotein drive antibody escape. *Science* (2021).
15. Andreano, E., *et al.* SARS-CoV-2 escape in vitro from a highly neutralizing COVID-19 convalescent plasma. *bioRxiv* (2020).

16. Greaney, A.J., *et al.* Complete Mapping of Mutations to the SARS-CoV-2 Spike Receptor-Binding Domain that Escape Antibody Recognition. *Cell Host Microbe* **29**, 44-57 e49 (2021).
17. Weisblum, Y., *et al.* Escape from neutralizing antibodies by SARS-CoV-2 spike protein variants. *Elife* **9**(2020).
18. Winkler, E.S., *et al.* SARS-CoV-2 infection of human ACE2-transgenic mice causes severe lung inflammation and impaired function. *Nat Immunol* **21**, 1327-1335 (2020).
19. Piccoli, L., *et al.* Mapping Neutralizing and Immunodominant Sites on the SARS-CoV-2 Spike Receptor-Binding Domain by Structure-Guided High-Resolution Serology. *Cell* **183**, 1024-1042 e1021 (2020).
20. Wolfel, R., *et al.* Virological assessment of hospitalized patients with COVID-2019. *Nature* **581**, 465-469 (2020).
21. Nielsen, M., *et al.* Reliable prediction of T-cell epitopes using neural networks with novel sequence representations. *Protein Sci* **12**, 1007-1017 (2003).
22. Duchene, S., *et al.* Temporal signal and the phylodynamic threshold of SARS-CoV-2. *Virus Evol* **6**, veaa061 (2020).
23. Kemp, S.A., *et al.* SARS-CoV-2 evolution during treatment of chronic infection. *Nature* (2021).
24. Daoud, A., *et al.* Immunosuppression in kidney transplant recipients with COVID-19 infection - where do we stand and where are we heading? *Ren Fail* **43**, 273-280 (2021).
25. Cele, S., *et al.* Escape of SARS-CoV-2 501Y.V2 from neutralization by convalescent plasma. *Nature* (2021).
26. Collier, D.A., *et al.* Sensitivity of SARS-CoV-2 B.1.1.7 to mRNA vaccine-elicited antibodies. *Nature* (2021).
27. Wang, P., *et al.* Antibody Resistance of SARS-CoV-2 Variants B.1.351 and B.1.1.7. *Nature* (2021).
28. Su, Y.C.F., *et al.* Discovery and Genomic Characterization of a 382-Nucleotide Deletion in ORF7b and ORF8 during the Early Evolution of SARS-CoV-2. *mBio* **11**(2020).
29. Pfefferle, S., *et al.* Reverse genetic characterization of the natural genomic deletion in SARS-Coronavirus strain Frankfurt-1 open reading frame 7b reveals an attenuating function of the 7b protein in-vitro and in-vivo. *Virol J* **6**, 131 (2009).
30. Johnson, B.A., *et al.* Loss of furin cleavage site attenuates SARS-CoV-2 pathogenesis. *Nature* **591**, 293-299 (2021).

Methods

Case history. A patient in his 50´swas hospitalized at the University Medical Center, Freiburg, Germany for 7 monthHe underwent an organ transplantation and was treated with diverse regimens of immunosuppression, consisting of tacrolimus (4 mg/day), mycophenolat mofetil (2 mg/day) and prednisone (10 mg/day) (see figure 1). The patient received five days ivermectin treatment (33 mg/day) and later a ten days Remdesivir treatment (200 mg on day 1, 100 mg/day 2 to 10).

Ethical statements. The project has been approved by the University Medical Center, Freiburg, ethical committee. Written informed consent was obtained from all participants and the study was conducted according to federal guidelines, local ethics committee regulations (Albert-Ludwigs-Universität, Freiburg, Germany: No. F-2020-09-03-160428 and no. 322/20) and the Declaration of Helsinki (1975). All routine virological laboratory testing of patient specimens was performed in the Diagnostic Department of the Institute of Virology, University Medical Center, Freiburg (Local ethics committee no. 1001913).

Virus detection by qRT-PCR. SARS-CoV-2 RNA testing of respiratory tract samples was performed using the RealStar SARS-CoV-2 RT-PCR kit (Altona Diagnostics, Hamburg, Germany). RNA samples were extracted using QIAamp MinElute Virus Spin kit (Qiagen, Hilden, Germany). Tests were performed and interpreted according to the manufacturer's instructions and semi-quantitative results reported in cycle threshold (Ct) values.

Serological testing. Convalescent sera of COVID-19 patients and sera from vaccinees after the second dose of the BNT162b2 mRNA vaccine (Pfizer/BioNTech) were obtained from the Hepatology-Gastroenterology-Biobank as part of the Freeze-Biobank Consortium at the University Medical Center Freiburg. Written informed consent was obtained from all blood donors prior to inclusion.

SARS-CoV-2 specific anti-spike protein (S1) IgG (Euroimmun, Medizinische Labordiagnostika AG, Lübeck, Germany) and anti-nucleoprotein (N) IgG ELISA (Mikrogen Diagnostik GmbH, Neuried, Germany) were performed according to manufacturer's protocol. Results were evaluated semi-quantitatively as arbitrary units (AU) compared to the manufacturer's calibrators.

To determine the SARS-CoV-2-specific antibodies in mouse sera, VeroE6 cells in 96-well plates were infected with the prototypic Muc-IMB-1virus isolate (kindly provided by Roman Woelfel, Bundeswehr Institute of Microbiology[20]). Fixed and permeabilized cells were incubated with dilutions of the post-infectious mouse sera and SARS-CoV-2-specific antibodies were detected by fluorescence-labeled secondary anti-mouse IgG antiserum. The serum dilution giving a clear fluorescence signal in the infected cells was interpreted as positive.

For the SARS-CoV-2 neutralization plaque reduction assay, serial serum dilutions were incubated with 100 plaque forming units (pfu) for 1 hour. The mixture was dispersed on VeroE6 cells in 12-well format and the cells were overlaid with 0.6% Oxoid-agar for 48 h at 37°C. The fixed cells were stained with Crystal violet. Number of plaques was compared with an untreated control without serum.

For the detection of neutralizing antibodies by indirect immunofluorescence, 400 pfu of SARS-CoV-2 were preincubated with serially diluted serum samples for 1h and the mixture was used to infect VeroE6 cells in 96-well plates. For each sample, one control without serum was included. Cells were fixed 20 h post infection and stained with anti-SARS-CoV nucleocapsid (N) rabbit antiserum (#200-401-A50, Rockland Immunochemicals). The plates were evaluated by fluorescence microscopy. The highest dilution of the serum that showed less than 50% of infected cells compared to a non-reactive control serum was classified as neutralization titer.

SARS-CoV-2 S1-specific T cell response. The S1 amino-acid sequence of SARS-CoV-2 (GenBank: MN908947.3) was analyzed for *in silico* prediction of peptide binding with ANN 4.0 on the Immune Epitope Database website[21]. The HLA-A*02:01-restricted 9-mer peptide, $S_{133-141}$ FQFCNDPF*L*, and the HLA-A*03:01-restricted 9-mer peptide, $S_{142-150}$ GVYYHKNNK, both overlapping with del141-144, the HLA-A*02:01-restricted 10-mer peptide, $S_{244-247}$ TLLALHRSYL, overlapping with del244-247, as well as a HLA-A*03:01-restricted 9-mer peptide, $S_{378-386}$

KCYGVSPTK, of the S1 domain were selected and synthesized for further analysis. Subsequently, PBMCs ($1-2 \times 10^6$) of the convalescent immunosuppressed COVID-19 patient and of four HLA-A*02:01/HLA-A*03:01 positive SARS-CoV-2 convalescent immunocompetent donors were stimulated with these peptides (5 µM) and anti-CD28 mAb (0.5 µg ml^{-1}, BD Biosciences) and expanded for 14 days in complete RPMI culture medium containing rIL2 (20 IU ml^{-1}, Miltenyi Biotec). IFNγ production was assessed after a 5h re-stimulation with the respective peptide [31].

Cell culture. Virus isolation, cell culture and mouse infection experiments with SARS-CoV-2 were performed under Biosafety Level 3 (BSL3) protocols at the Institute of Virology, Freiburg, approved by the Regierungspraesidium Tuebingen (No. 25-27/8973.10-18 and UNI.FRK.05.16-29). Filtered throat swab samples were inoculated on African green monkey kidney VeroE6 cells (ATCC CRL-1586) (2 x 10^6 cells) in 4 ml DMEM with 2% FCS and incubated at 37°C and 5% CO2 for 4 to 6 days until cytopathic effect was visible. The culture supernatant was cleared and stored at -80°C. Virus titers were determined by plaque assay on VeroE6 cells.

For neutralization assays we used established prototypic isolates: Muc-IMB-1, lineage B.1[20]; UK variant B.1.1.7 (hCoV-19/Germany/NW-RKI-I-0026/2020; ID: EPI_ISL_751799) and South African variant B.1.351 (hCoV-19/Germany/NW-RKI-I-0029/2020; ID: EPI_ISL_803957).

VeroE6 or human bronchial epithelium Calu-3 cells (ATCC-HTB-55) in 6-well plates, 1 x 10^6 cells, were infected with a moi of 0.001 for 1.5h. Cells were washed three times with PBS and overlaid with 2 mL DMEM with 2% FCS. The supernatants were taken at different time points after infection and titers were determined by plaque assay. For viral protein analysis, the cells were lysed with tissue protein extraction reagent (T-PER; Thermo Fisher Scientific), separated by 10% SDS-polyacrylamid gel electrophoresis and transferred on PVDF membranes. The membranes were stained with the SARS-CoV-2 N-specific, SARS-CoV-2 spike protein (RBD)-specific (200-401-A50 and 600-401-MS8, Rockland) or actin-specific (A5060, Sigma) rabbit antisera. Detection of the primary antibodies was performed with fluorescent-labeled (Li-COR) secondary antibodies.

Immunofluorescence analysis. VeroE6 cells seeded on glass coverslips were infected with SARS-CoV-2 isolates at a moi of 0.1. At 8 hours post infection, cells were fixed in 4% paraformaldehyde, permeabilized with 0.3% Triton X-100 and blocked in 10% fetal calf serum. SARS-CoV-2 N- and spike-specific primary antibodies and AF568-labeled goat-anti-rabbit (Invitrogen, #A11011, 1:400) secondary antibody as well as AF488-labeled Phalloidin (Hypermol, #8813-01, 1:250) were used for staining. The coverslips were embedded in Diamond Antifade Mountant with 4′,6-diamidino-2-phenylindole (DAPI) (ThermoFisher, #P36971). Fluorescence images were generated using a LSM800 confocal laser-scanning microscope (Zeiss) equipped with a 63X, 1.4 NA oil objective and Airyscan detector and processed with Zen blue software (Zeiss) and ImageJ/Fiji.

Virus pseudotype VSV*ΔG(FLuc) neutralization assay. cDNAs encoding the S protein were prepared from oropharyngeal swab samples of the COVID-19 patient obtained at days d14 and d105 and were cloned into the eukaryotic expression vector pCAGGS[32]. Single and double spike mutations were introduced into the pCAGGS-S(d14) construct. BHK-21 cells were transfected with the pCAGGS-S plasmids and later inoculated with 5 ffu/cell of VSV*ΔG(FLuc), coding for firefly luciferase, as described[33]. Cells were incubated in medium containing the monoclonal mAb I1 antibody (ATCC) directed against VSV-G. The supernatants containing the pseudotype viruses were harvested and stored at -70°C.

The pseudotyped virus neutralization test was performed as described recently[34]. Pseudotyped VSV*ΔG(FLuc) (200 ffu) were preincubated with twofold serial dilutions of convalescent sera in DMEM cell culture medium. The virus/serum mixture was transferred to VeroE6 cells in 96-well plates and incubated for 16 hours at 37°C. Thereafter, the cells were lysed and firefly luciferase activity was determined using ONE-GloTM substrate (Promega) and a GloMax® plate reader (Promega). The reciprocal antibody dilution causing 50% reduction of the luminescence signal was calculated and expressed as neutralization titer 50% (NT_{50}).

Infection of K18-hACE2 transgenic mice. Transgenic (K18-hACE2)2Prlmn mice[18] were purchased from The Jackson Laboratory and bred locally. Hemizygous 8-12-week-old animals of both sexes were

used in accordance with the guidelines of the Federation for Laboratory Animal Science Associations and the National Animal Welfare Body. All experiments were in compliance with the German animal protection law and approved by the animal welfare committee of the Regierungspraesidium Freiburg (permit G-20/91).

Mice were anesthetized using isoflurane and infected intranasally (i.n.) with virus dilutions in 40 µl PBS containing 0.1 % BSA. Mice were monitored daily and euthanized if severe symptoms were observed or body weight loss exceeded 25 % of the initial weight. Serum samples were collected from the vena facialis. SARS-CoV-2 specific antibody titers were determined by indirect immunofluorescence as described above.

Whole genome sequencing. cDNA was produced from extracted RNA of oropharyngeal swab samples using random hexamer primers and Superscript III (ThermoFisher) followed by a PCR tiling the entire SARS-CoV-2 genome (ARTIC V3 primersets; https://github.com/artic-network/artic-ncov2019). This produced 400 bp long, overlapping amplicons that were subsequently used to prepare the sequencing library. Briefly, the amplicons were cleaned with AMPure magnetic beads (Beckman Coulter). Afterwards the QIAseq FX DNA Library Kit (Qiagen) was used to prepare indexed paired end libraries for Illumina sequencing. Normalized and pooled sequencing libraries were denatured with 0.2 N NaOH. This 9 pM library was sequenced on an Illumina MiSeq instrument using the 300-cycle MiSeq Reagent Kit v2.

For sequencing of virus stocks produced in cell culture, RNA was extracted with the Quick-RNA Viral Kit (Zymo Research) and paired end libraries without a previous PCR amplification were prepared using the TruSeq Stranded Total RNA Kit (Illumina). A total of 10 pM library was sequenced on the Illumina MiSeq instrument.

The de-multiplexed raw reads were subjected to a custom Galaxy pipeline, which is based on bioinformatics pipelines on usegalaxy.eu (doi: 10.5281/zenodo.3685264)[35]. The raw reads were pre-processed with fastp (https://www.biorxiv.org/content/10.1101/274100v2) and mapped to the SARS-CoV-2 Wuhan-Hu-1 reference genome (Genbank: NC_045512) using BWA-MEM (https://academic.oup.com/bioinformatics/article/25/14/1754/225615). For datasets, which were

produced with the ARTIC v3 protocol, primer sequences were trimmed with ivar trim (https://andersen-lab.github.io/ivar/html/manualpage.html). Variants (SNPs and INDELs) were called with the ultrasensitive variant caller LoFreq (https://academic.oup.com/nar/article/40/22/11189/1152727), demanding a minimum base quality of 30 and a coverage of at least 5-fold. Afterwards, the called variants were filtered based on a minimum variant frequency of 10 % and on the support of strand bias. The effects of the mutations were automatically annotated in the vcf files with SnpEff (https://www.tandfonline.com/doi/full/10.4161/fly.19695). Finally, consensus sequences were constructed by bcftools (https://academic.oup.com/bioinformatics/article/25/16/2078/204688). Regions with low coverage or variant frequencies between 30 and 70 % were masked with Ns. The final consensus sequences have been deposited in the GISAID database (www.gisaid.org) (Extended data table 2).

Phylogenetic and variant analysis. All available sequences from Germany deposited in GISAID (http://gisaid.org/) between February and April 2020 were downloaded (as of 11th of February 2021) and 250 sequences randomly subsampled excluding sequences already deposited by the Virology in Freiburg (Extended data table 3). For the phylogenetic analysis, the sequences were first aligned with MAFFT (v7.45)[36] and a tree was constructed with IQ-Tree (v2.1.2)[37]. The best fitting substitution model was automatically determined and the tree was calculated with 1000 bootstrap replicates. Branch support was approximated using the Shimodaira–Hasegawa [SH]-aLRT method (1000 replicates). The tree was rooted to the reference sequence NC_045512. The clades were classified with the webservers of Nextclade (clades.nextstrain.org) and Pangolin (pangolin.cog-uk.io). To visualize the phylogenetic tree a custom R script was written utilizing the ggtree (v2.2.4) (https://academic.oup.com/mbe/article-abstract/35/12/3041/5142656), treeio (v1.12.0) (https://academic.oup.com/mbe/article-abstract/37/2/599/5601621) and ggplot2 (v3.3.3) packages (https://link.springer.com/chapter/10.1007/978-3-319-24277-4_12). An in-house R script was also used to plot the variant frequencies that were detected by LoFreq as a heatmap (pheatmap package v1.0.12). Both scripts are publicly available (github.com/jonas-fuchs/SARS-CoV-2-analyses) and the variant frequency plot has been implemented as a galaxy tool (Variant Frequency Plot on usegalaxy.eu).

Visualization of the spike protein structure. The EM structure of the closed conformation of D614G SARS-CoV-2 spike protein was loaded from the protein data bank (10.2210/pdb7BNM/pdb) and visualized with UCSF ChimeraX version: 1.1 (2020-09-09).

Data availability. All necessary data and informations are given in the manuscript. The sequence data are submitted to GISAID data base and are publicly available (Extended data table 2). Further additional informations about the patient will not be shared due to protection of individuals‘ privacy.

Code availability. The scripts are publicly available (github.com/jonas-fuchs/SARS-CoV-2-analyses) and the variant frequency plot has been implemented as a galaxy tool (Variant Frequency Plot on usegalaxy.eu).

Additional References

31. Wieland, D., *et al.* TCF1(+) hepatitis C virus-specific CD8(+) T cells are maintained after cessation of chronic antigen stimulation. *Nat Commun* **8**, 15050 (2017).
32. Niwa, H., Yamamura, K. & Miyazaki, J. Efficient selection for high-expression transfectants with a novel eukaryotic vector. *Gene* **108**, 193-199 (1991).
33. Berger Rentsch, M. & Zimmer, G. A vesicular stomatitis virus replicon-based bioassay for the rapid and sensitive determination of multi-species type I interferon. *PLoS One* **6**, e25858 (2011).
34. Zettl, F., *et al.* Rapid Quantification of SARS-CoV-2-Neutralizing Antibodies Using Propagation-Defective Vesicular Stomatitis Virus Pseudotypes. *Vaccines (Basel)* **8**(2020).
35. Jalili, V., *et al.* The Galaxy platform for accessible, reproducible and collaborative biomedical analyses: 2020 update. *Nucleic Acids Res* **48**, W395-W402 (2020).
36. Katoh, K. & Standley, D.M. MAFFT multiple sequence alignment software version 7: improvements in performance and usability. *Mol Biol Evol* **30**, 772-780 (2013).
37. Nguyen, L.T., Schmidt, H.A., von Haeseler, A. & Minh, B.Q. IQ-TREE: a fast and effective stochastic algorithm for estimating maximum-likelihood phylogenies. *Mol Biol Evol* **32**, 268-274 (2015).

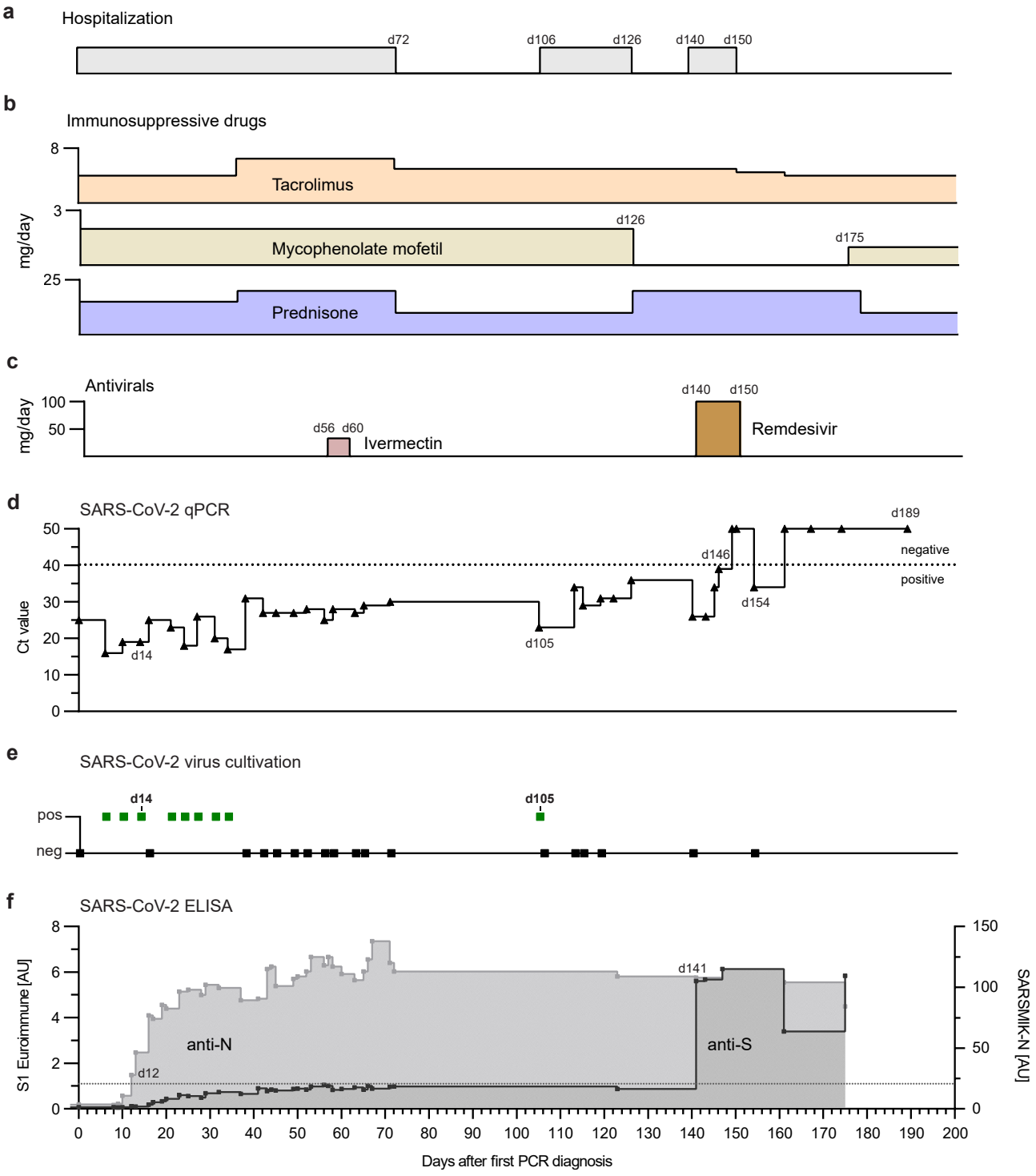

Fig. 1 Summary of the clinical course of the SARS-CoV-2-positive kidney transplant patient. Temporal overview of (a) hospitalization, (b) immunosuppressive treatment (daily dose in mg/day) and (c) antiviral therapy (daily dose in mg/day), Remdesivir was given 200 mg on the first day and 100 mg/day 2 to 10. (d) Diagnostic SARS-CoV-2 RT-qPCR cycle threshold (Ct) values of oropharyngeal swabs over time. Day 0 indicates the first positive RT-qPCR result, 12 days after kidney transplantation. The dotted line indicates the cutoff value (Ct ≥ 40) between positive and negative results. (e) Attempts of virus isolation from oropharyngeal swabs. (f) Detection of spike S1-subunit- and nucleoprotein (N) specific antibodies by ELISA. The dotted line indicates the anti-S1 ELISA cutoff at 1.1 arbitrary unit (AU).

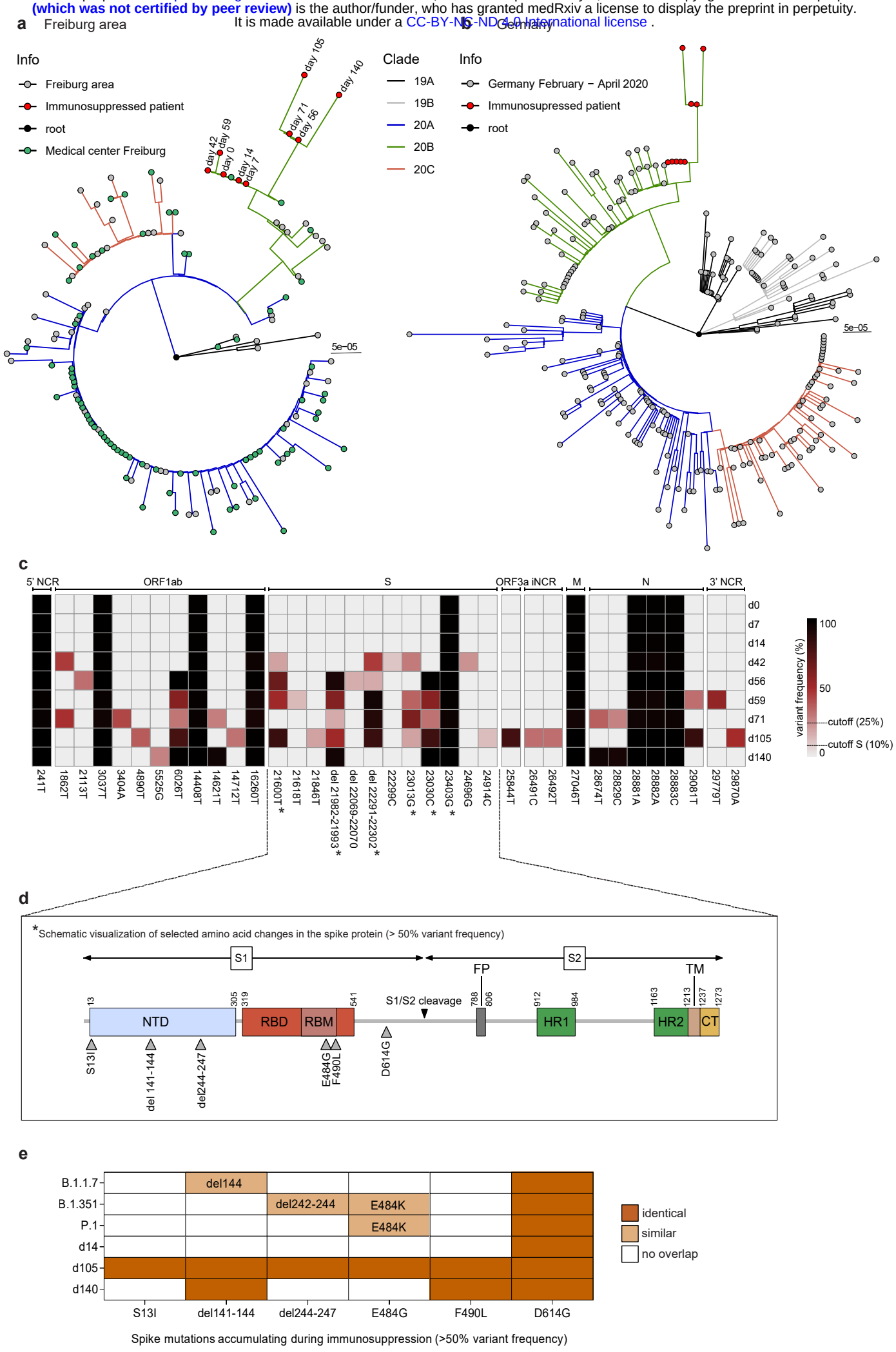

Fig. 2 SARS-CoV-2 whole genome sequencing and phylogenetic analysis. Phylogenetic analysis of the viral sequences obtained from patient swabs between day 0 to day 140, after the first positive RT-qPCR result. (Fig.2 continued on the following page)

Fig. 2 continued: The sequences were aligned to a set of representative SARS-CoV-2 genomic sequences from the Freiburg area (a) and from Germany (b) that were obtained in spring 2020 and have been deposited in the GISAID data bank (Extended data table 2 and 3). The circularized maximum-likelihood phylogenetic tree was constructed with IQ-Tree (GTR+F+I) and rooted on the Wuhan-Hu-1 reference sequence (NC_045512). The sequences obtained from the immunosuppressed patient are indicated as red dots. The scale represents nucleotide substitutions per site. (c) Schematic overview of the viral genome variations from patient swab samples (day 0-140) in comparison to the Wuhan-Hu-1 reference sequence. The heatmap summarizes the positions in the viral genome and the variant frequencies in the different samples (cut off values of 25% and 10% for the S gene analysis, respectively). The days of sampling are indicated at the right and the heatmap color intensity indicates variant frequencies. Stars denote non-synonymous mutations leading to amino acid substitutions in the spike protein (> 50 % of reads). (d) Schematic overview of the SARS-CoV-2 spike protein including the S1 and S2 cleavage products and functional domains such as the N-terminal domain (NTD), receptor-binding domain (RBD), receptor binding motif (RBM), S1/S2 proteolytic furin cleavage site, fusion peptide (FP), heptad repeat regions (HR1/HR2), transmembrane domain (TM) and C-terminal domain (CT). Selected non-synonymous changes in the spike (S) gene from panel c are indicated. (e) Summary of mutations found in the spike protein of the patient sequences obtained on d14, d105 and d140 (>50 % of reads) in comparison to circulating new variants of concern from the UK, B.1.1.7[3], South Africa, B.1.351[4] and Brazil, P.1[5].

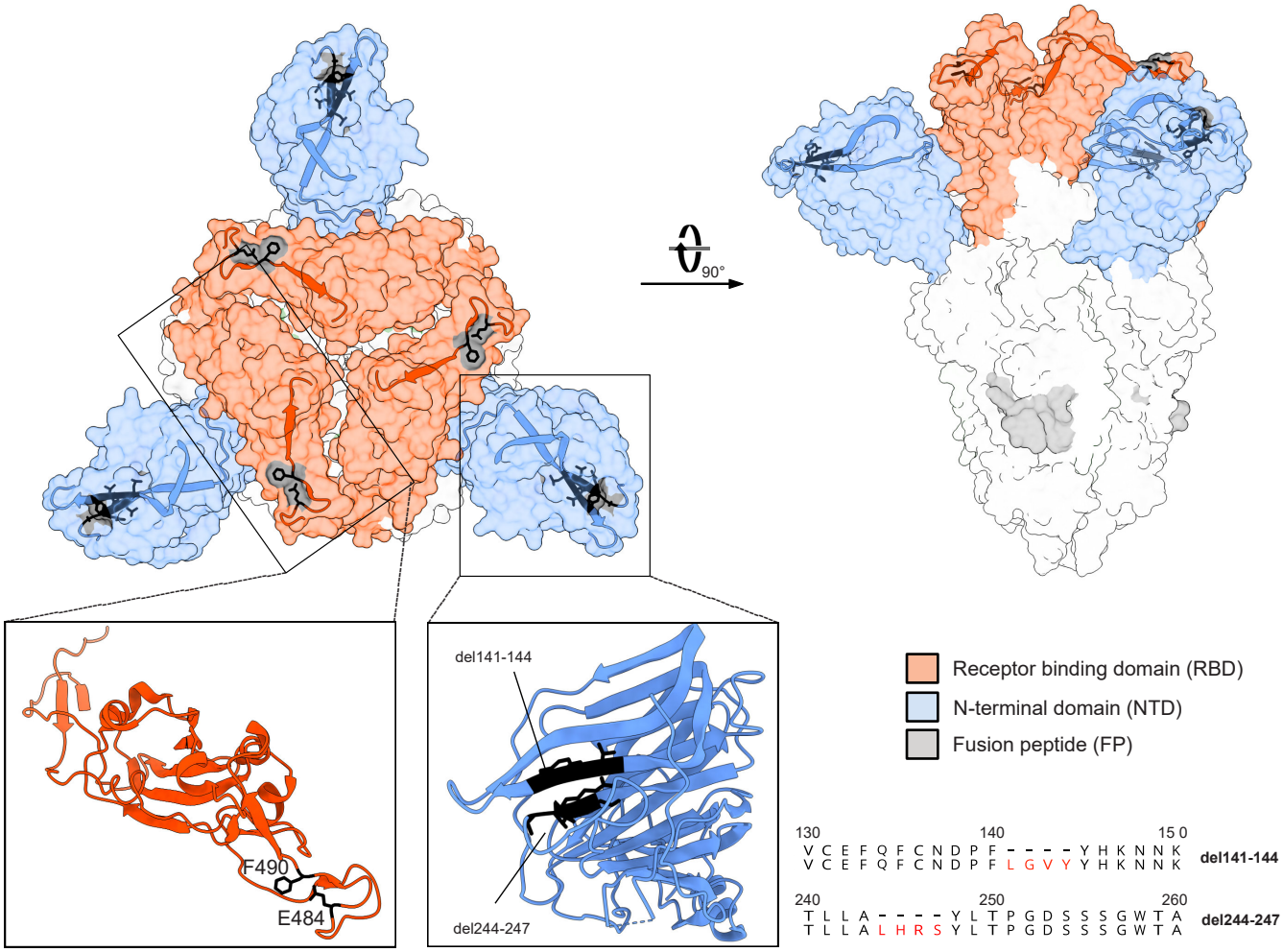

Fig. 3 Structure of the SARS-CoV-2 spike trimer. The spike structure (PDB accession number: 7BNM) with the most prominent mutations in the patient viral sequences is shown in surface presentation. The NTD is colored in blue, the RBD in red and the fusion peptide in gray. Close-ups of the single NTD and RBD regions defined by boxes are presented as ribbons. The location of the deletions in the NTD and amino acid substitutions in the RBD are indicated by black residues. Furthermore, the deletions in the NTD are displayed as amino acid alignments at the right.

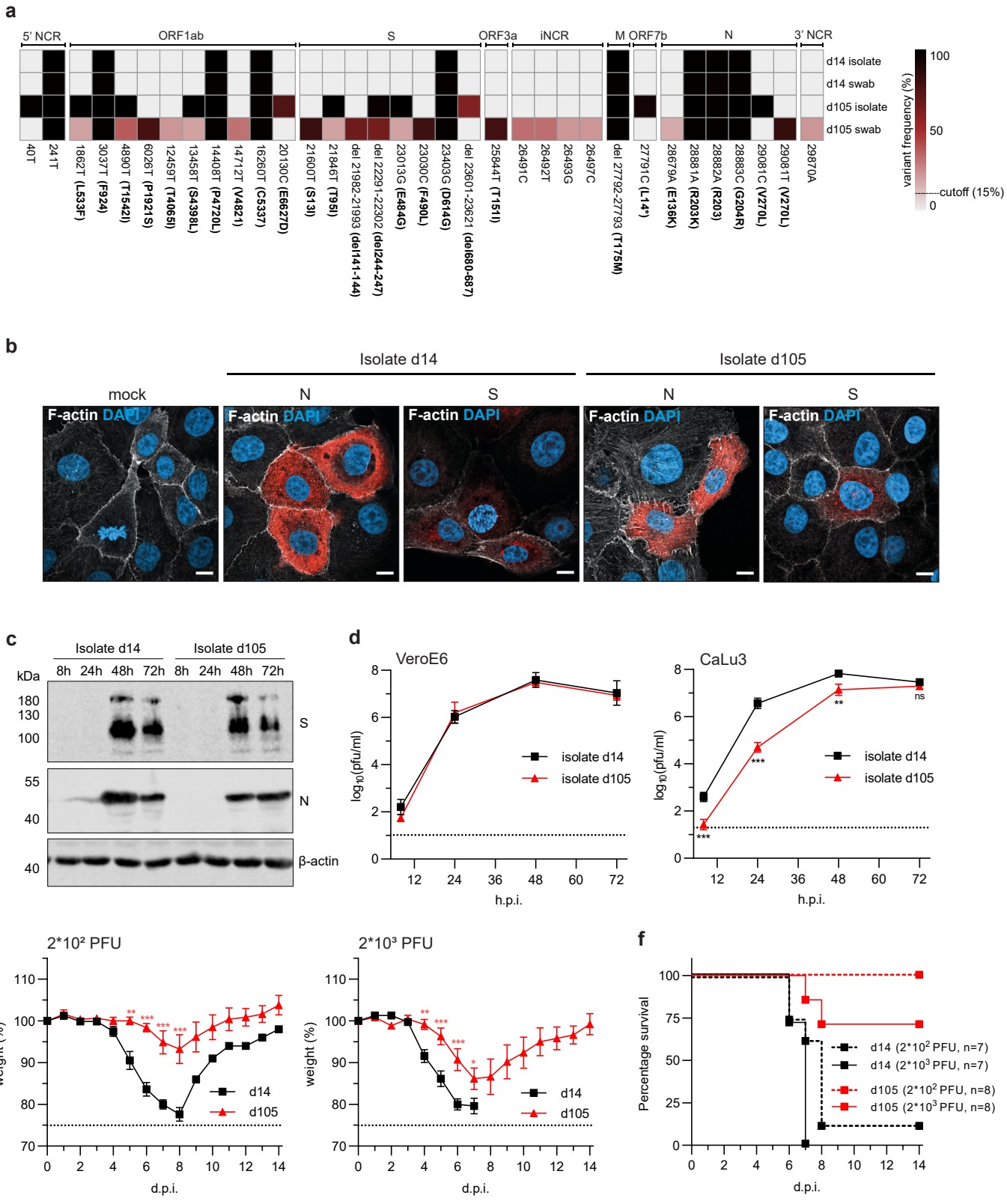

Fig. 4 The late SARS-CoV-2 isolate with deletions in the spike protein is attenuated. (**a**) Schematic overview of the sequence variations in SARS-CoV-2 genomes detected in early (d14) or late (d105) swab samples and isolated viruses. The heatmap illustrates the positions and the frequency of major variations in the viral genome (cut off 15%). The days of isolation are indicated at the right. The heatmap colors represent the variant frequencies. In ORF7b, L14* indicates a frame shift mutation due to a deletion of two nucleotides. (**b**) Immunofluorescence analysis of SARS-CoV-2 infected cell cultures. VeroE6 cells were infected with one of the two virus isolates (d14 or d105) using a multiplicity of infection (moi) of 0.1 plaque forming units (pfu)/cell. At 8 h post infection, the cells were fixed and stained with SARS-CoV-2 N- and S-specific antibodies (red). In addition, F-actin (white) and nuclear DNA (DAPI, blue) were detected. (**c**) Western blot analysis of viral protein expression. Calu-3 cells were infected with a moi of 0.001 pfu/cell with either of the two virus isolates (d14 or d105). Cells were lysed 8h, 24h, 48h and 72h post-infection and analyzed using N- and S-specific antibodies. Detection of β-actin was used as loading control. (Fig.4 continued on the following page)

Fig. 4 continued: (**d**) Growth of the two patient isolates in VeroE6 and Calu-3 cells. The cells were infected with either of the two patient isolates (d14 or d105) using a moi of 0.001 pfu/cell. At different time points post infection, cell culture supernatants were collected and viral titers were determined by plaque assay on VeroE6 cells. The log-transformed titers are shown as means ± SD of results from three independent experiments. Significance was determined via two-way ANOVA with a Sidak´s multiple comparison test, **p<0.0021, ***p<0.0002, ns=non significant. (E and F) Late SARS-CoV-2 isolate is attenuated in mice. Weight loss (**e**) and survival (**f**) of 8 to 12 weeks-old K18-hACE2 mice intranasally infected with 200 or 2000 pfu of d14 or d105 viruses. Signs of disease and body weight loss were monitored daily for 14 days. The weight loss is visualized as mean ± SEM. Significance was determined via two-way ANOVA with a Sidak´s multiple comparison test, *p<0.0332, **p<0.0021, ***p<0.0002.

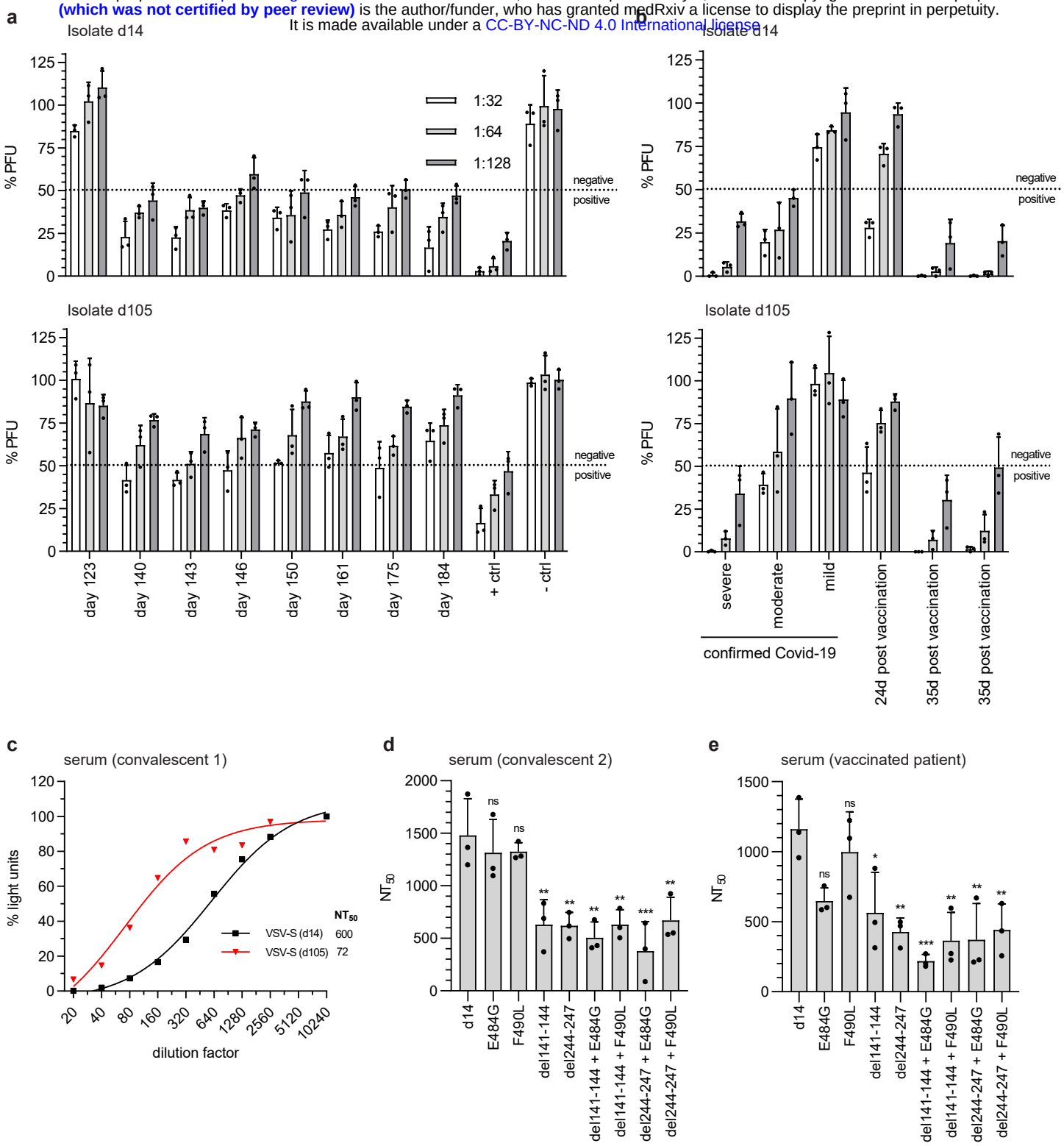

Fig. 5 Delayed seroconversion and viral escape from the spike protein-specific antibody response. (**a** and **b**) Detection of neutralizing activity of immune sera against SARS-CoV-2 variants. 100 pfu of the d14 and d105 isolates were incubated for 60 min at room temperature with serial dilutions of the patient sera. Sera obtained from naïve (– ctrl) or convalescent individuals (+ ctrl) served as negative and positive controls. Virus neutralization was determined by plaque assay on VeroE6 cells. Virus titers are indicated as percentages (mean ±SD) of the titer of the untreated virus inoculum. The dotted lines indicate the cutoff value between positive (<50%) and negative (>50%) neutralization. (**a**) Sera from the immunocompromised patient. The times of blood withdrawal are indicated. (**b**) Convalescent sera from COVID-19 patients suffering from mild, moderate or severe disease or human post vaccination (BNT162b2 mRNA) sera. (**c-e**) Neutralization capacity of SARS-CoV-2 antisera using VSV*ΔG(FLuc) vector pseudotyped with the SARS-CoV-2 spike protein and coding for firefly luciferase. The pseudotyped viruses were incubated with serial dilutions of a COVID-19 convalescent serum prior to inoculation of VeroE6 cells. Pseudotyped virus infection was monitored 16 h post infection by measuring the firefly luciferase activity in the cell lysates. (**c**) Neutralization of VSV*ΔG(FLuc) pseudotyped with the early and late SARS-CoV-2 spike variants (d14 and d105) using serial dilutions of a COVID-19 convalescent serum. (**d** and **e**) Neutralization of VSV*ΔG(FLuc) pseudotyped with the d14 spike protein containing the individual or combined mutations characteristically found in the late d105 and d140 variants. Immune serum from a convalescent COVID-19 patient (**d**) or a vaccinated person (**e**) were analyzed. The neutralization was determined by calculating the NT_{50} via a non-linear regression (variable slope, four parameters). Shown are means ± SD (n=3). Statistics were calculated with a one-way ANOVA (Tukey's multiple comparison test), ns = non-significant, *p<0.0332, **p<0.0021, ***p<0.0002.

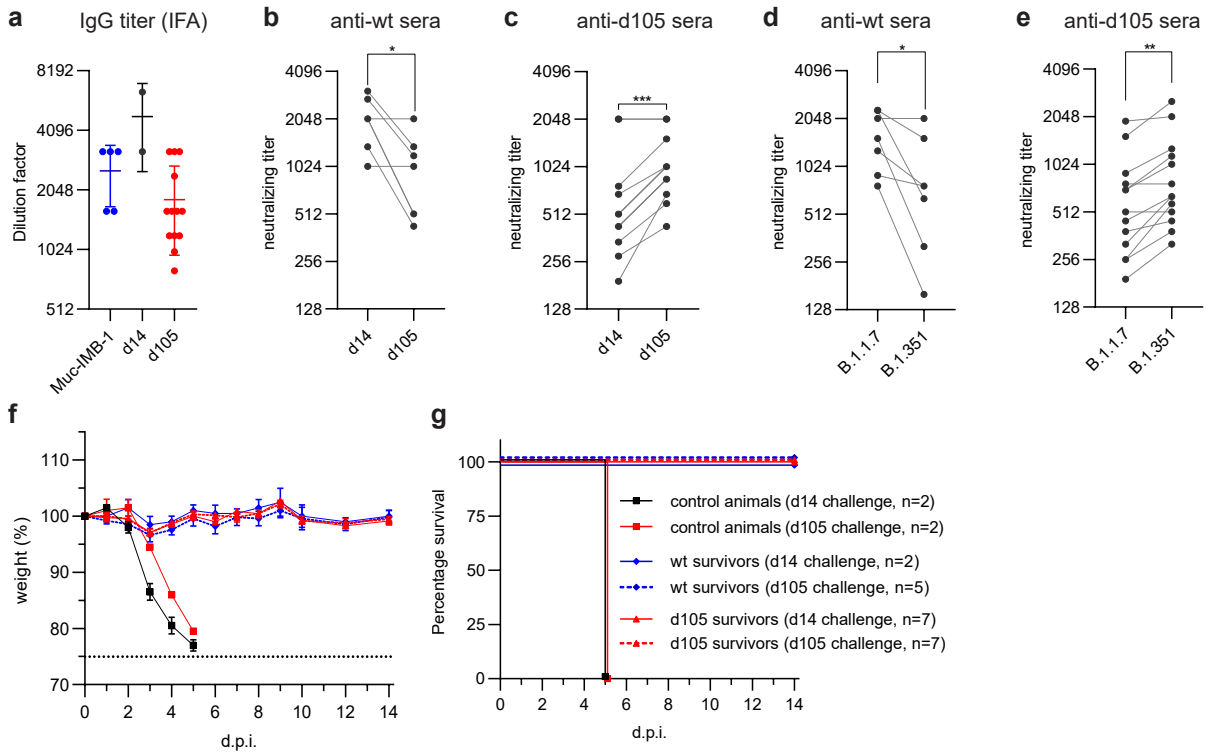

Fig. 6 Late SARS-CoV-2 isolate elicits cross-reactive protective immunity in mice. Sera were collected from convalescent K18-hACE2 mice at least 21 days post infection with Muc-IMB-1 (n=5), d14 (n=2) or d105 (n=13) virus isolates. (**a**) Anti-SARS-CoV-2 IgG titers of serially diluted sera (mean ±SD) were determined using virus-infected cells and indirect immunofluorescence analysis (IFA). (**b** and **c**) Neutralization of d14 and d105 virus isolates by convalescent mouse sera obtained after infection with wild-type SARS-CoV-2, d14 and Muc-IMB-1 (anti-wt sera, n=7) (**b**), or with variant d105 virus isolate (anti-d105 sera, n=13) (**c**). Neutralization capacity was determined by incubating 100 pfu of either virus isolate with serial dilutions of the mouse sera. The mixture was then applied to VeroE6 cells and infected cells were stained with N-specific antibodies. The highest dilution for each individual serum causing 50% neutralization was plotted as neutralizing titer. (**d** and **e**) Neutralization of B.1.1.7 and B.1.351 variants of concern by mouse convalescent sera was determined as described in panels b and c. 100 pfu of the variant viruses were incubated with dilutions of sera from mice infected with wild-type SARS-CoV-2 (wt) (**d**) or d105 isolate (**e**). Neutralization titers are meant as the highest dilution for each individual serum causing 50% reduction of infectivity. Each serum titer (b - e) is shown as mean out of two independent experiments. Significance was determined via a paired t test with *p<0.0332, **p<0.0021, ***p<0.0002. (**f** and **g**) Convalescent animals are protected against re-challenge infection. Weight loss (**f**) and survival (**g**) of convalescent K18-hACE2 mice (mean ± SEM), challenged one to four months after the prime infection. Animals primarily infected with d14 and Muc-IMB-1 viruses (pooled wt survivors, n=7), or with d105 virus (n=14) were intranasally challenged with 100,000 pfu of d14 or d105 viruses (2 to 7 mice per group, as indicated). As a control, naïve 8 weeks old K18-hACE2 mice were intranasally infected with 100,000 pfu of d14 or d105 isolate viruses (n=2 per group).

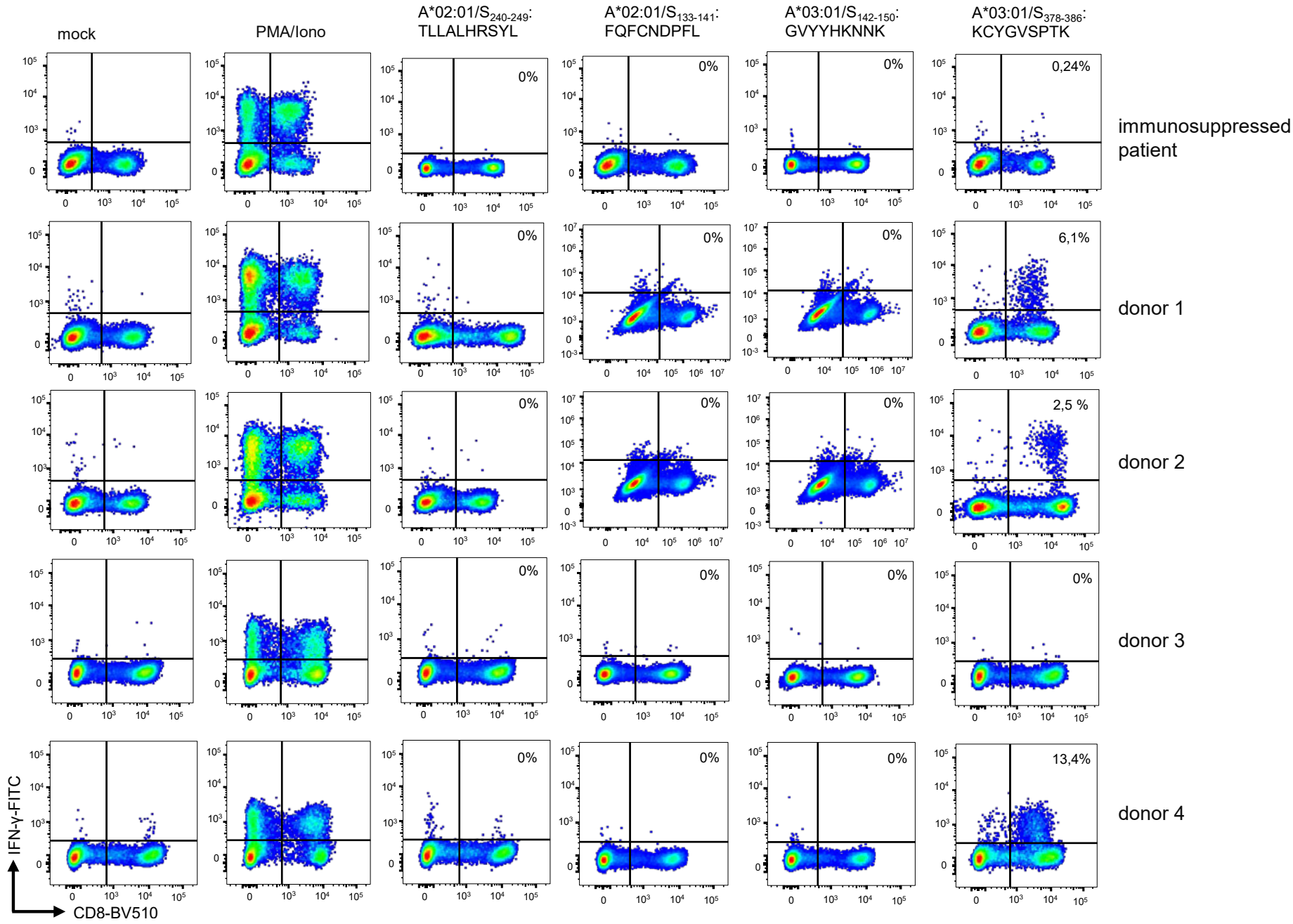

Extended Data Fig. 1 Lack of detectable CD8+ T cell responses targeting the mutated regions in the spike protein. HLA-A*02:01/HLA-A*03:01-restricted CD8+ T cell epitopes overlapping with the del141-144 and the del244-247 deletions as well as a control peptide 378-386 in the S1 domain were predicted *in silico*. Peptide-specific CD8+ T cell responses were assessed by intra-cellular IFN□ production following a 14-day *in vitro* peptide-specific CD8+ T cell expansion. CD8+ T cells targeting the *in silico*-predicted SARS-CoV-2 S1-specific, HLA-A*02:01/HLA-A*03:01-restricted CD8+ T cell epitopes were neither detectable in the convalescent, immunosuppressed COVID-19 patient (upper panel) nor in four additional HLA-A*02:01/HLA-A*03:01 positive convalescent, immunocompetent COVID-19 patients (donor 1 to 4). CD8+ T cell responses targeting the immunodominant A*03:01/$S_{378-386}$ epitope are depicted as positive control, as well as mock-stimulated and PMA/Ionomycin-stimulated cells.

Day	Ct	SARS-S1	SARSMIK-N	Virus isolation	NT (dilution factor)
-3		0.068	3.35		
-2		0.07	3.44		
0	25	0.07	3.61	negative	
6	16			positive	
8		0.073	3.26		
9		0.065	4.23		
10	19	0.075	10.9	positive	
12		0.119	27.9		
13		0.095	46.5		0
14	19			positive	
16	25	0.184	77	negative	
17		0.286	74.1		
19		0.332	85.5		
20		0.434	82.4		0
21	23			positive	
23		0.599	96.6		
24	18			positive	
25		0.561	98.1		
27	26			positive	
28		0.496	93.6		
29		0.685	102		
31	20			positive	
32		0.735	99.5		
34	17			positive	
37		0.659	89.4		
38	31			negative	
41		0.902	90.6		0
41		0.902	90.6		
42	27			negative	
43		0.782	115		0
44		0.846	117		
45	27	0.807	101	negative	
46	50				
49	27	0.878	107	negative	0
50		0.882	109		
52	28	0.841	113	negative	
53		0.986	125		
56	25	1.05	118	negative	
57		1.01	125		
58	28	0.83	117	negative	
60		0.878	111		
63	27	0.939	106	negative	
65	29	0.846	113	negative	
66		1.01	123		
67		0.889	138		0
71	30	0.966	120	negative	
72		0.984	113		0
105	23			positive	
106				negative	
113	34			negative	
115	29			negative	
119	31			negative	
122	31				
123		0.872	109		0
126	36				
140	26			negative	
141		5.61	108		64
143	29	5.68			64
145	34				
146	39				
147		6.13	95.6		64
149	50				
150	50				64
154	34			negative	
161	50	3.4	104		64
167	50				
174	50				
175		5.84	84.2		64
184					64
189	50				

Extended Data Table 1: Detailed list of the course of infection. The table specifies the days of hospitalization post first detection of SARS-CoV-2 infection, SARS-CoV-2 specific RT-qPCR Ct values from throat swabs, anti-S-specific ELISA (cutoff value of 0.8 to 1.1 AU), anti-N-specific ELISA (cutoff value of 24 AU), attempts for virus isolation from throat swabs on VeroE6 cells, and titers of neutralizing antibodies against the prototype Muc-IMB-1 reference strain [20].

GISAID Accession	Metadata	GISAID Accession	Metadata	GISAID Accession	Metadata
EPI_ISL_852733	Freiburg area	EPI_ISL_852720	Medical center Freiburg	EPI_ISL_852708	Freiburg area
EPI_ISL_852729	Freiburg area	EPI_ISL_852719	Medical center Freiburg	EPI_ISL_852707	Medical center Freiburg
EPI_ISL_852727	Medical center Freiburg	EPI_ISL_852718	Medical center Freiburg	EPI_ISL_852706	Freiburg area
EPI_ISL_852693	Freiburg area	EPI_ISL_852717	Freiburg area	EPI_ISL_852705	Freiburg area
EPI_ISL_852772	Medical center Freiburg	EPI_ISL_852771	Freiburg area	EPI_ISL_852704	Freiburg area
EPI_ISL_852784	Medical center Freiburg	EPI_ISL_852716	Medical center Freiburg	EPI_ISL_852703	Freiburg area
EPI_ISL_852781	Medical center Freiburg	EPI_ISL_852715	Medical center Freiburg	EPI_ISL_852702	Freiburg area
EPI_ISL_852778	Medical center Freiburg	EPI_ISL_852714	Freiburg area	EPI_ISL_852700	Freiburg area
EPI_ISL_852775	Medical center Freiburg	EPI_ISL_852713	Medical center Freiburg	EPI_ISL_852699	Freiburg area
EPI_ISL_852701	Medical center Freiburg	EPI_ISL_852712	Medical center Freiburg	EPI_ISL_852698	Medical center Freiburg
EPI_ISL_852765	Medical center Freiburg	EPI_ISL_852711	Medical center Freiburg	EPI_ISL_852697	Freiburg area
EPI_ISL_852792	Medical center Freiburg	EPI_ISL_852748	Medical center Freiburg	EPI_ISL_852696	Freiburg area
EPI_ISL_852773	Medical center Freiburg	EPI_ISL_852802	Medical center Freiburg	EPI_ISL_852695	Medical center Freiburg
EPI_ISL_852744	Freiburg area	EPI_ISL_852804	Freiburg area	EPI_ISL_852694	Freiburg area
EPI_ISL_852743	Freiburg area	EPI_ISL_852737	Freiburg area	EPI_ISL_852692	Freiburg area
EPI_ISL_852741	Medical center Freiburg	EPI_ISL_852801	Medical center Freiburg	EPI_ISL_852691	Medical center Freiburg
EPI_ISL_852738	Freiburg area	EPI_ISL_852785	Medical center Freiburg	EPI_ISL_852690	Medical center Freiburg
EPI_ISL_852731	Freiburg area	EPI_ISL_852786	Medical center Freiburg	EPI_ISL_852769	Medical center Freiburg
EPI_ISL_852723	Freiburg area	EPI_ISL_852783	Medical center Freiburg	EPI_ISL_852689	Freiburg area
EPI_ISL_852710	Medical center Freiburg	EPI_ISL_852800	Medical center Freiburg	EPI_ISL_852688	Medical center Freiburg
EPI_ISL_852811	Freiburg area	EPI_ISL_852799	Medical center Freiburg	EPI_ISL_852687	Freiburg area
EPI_ISL_852732	Medical center Freiburg	EPI_ISL_852795	Medical center Freiburg	EPI_ISL_852686	Medical center Freiburg
EPI_ISL_852782	Medical center Freiburg	EPI_ISL_852790	Medical center Freiburg	EPI_ISL_852685	Freiburg area
EPI_ISL_852759	Medical center Freiburg	EPI_ISL_852774	Medical center Freiburg	EPI_ISL_852684	Medical center Freiburg
EPI_ISL_852758	Medical center Freiburg	EPI_ISL_852770	Medical center Freiburg	EPI_ISL_852683	Freiburg area
EPI_ISL_852812	Freiburg area	EPI_ISL_852779	Medical center Freiburg	EPI_ISL_852682	Medical center Freiburg
EPI_ISL_852755	Medical center Freiburg	EPI_ISL_852668	Medical center Freiburg	EPI_ISL_852810	Medical center Freiburg
EPI_ISL_852754	Medical center Freiburg	EPI_ISL_852798	Medical center Freiburg	EPI_ISL_852681	Medical center Freiburg
EPI_ISL_852749	Freiburg area	EPI_ISL_852797	Medical center Freiburg	EPI_ISL_852680	Medical center Freiburg
EPI_ISL_852747	Freiburg area	EPI_ISL_852796	Medical center Freiburg	EPI_ISL_852679	Medical center Freiburg
EPI_ISL_852746	Freiburg area	EPI_ISL_852793	Medical center Freiburg	EPI_ISL_852678	Freiburg area
EPI_ISL_852745	Freiburg area	EPI_ISL_852788	Medical center Freiburg	EPI_ISL_852677	Freiburg area
EPI_ISL_852742	Freiburg area	EPI_ISL_852760	Freiburg area	EPI_ISL_852676	Freiburg area
EPI_ISL_852803	Medical center Freiburg	EPI_ISL_852757	Freiburg area	EPI_ISL_852806	Immunosuppressed patient (day 140)
EPI_ISL_852740	Freiburg area	EPI_ISL_852756	Freiburg area	EPI_ISL_852809	Immunosuppressed patient (day 56)
EPI_ISL_852794	Medical center Freiburg	EPI_ISL_852753	Freiburg area	EPI_ISL_852807	Immunosuppressed patient (day 105)
EPI_ISL_852791	Medical center Freiburg	EPI_ISL_852752	Freiburg area	EPI_ISL_852805	Immunosuppressed patient (day 71)
EPI_ISL_852789	Medical center Freiburg	EPI_ISL_852751	Freiburg area	EPI_ISL_852808	Immunosuppressed patient (day 59)
EPI_ISL_852787	Medical center Freiburg	EPI_ISL_852750	Freiburg area	EPI_ISL_852667	Immunosuppressed patient (day 14)
EPI_ISL_852734	Medical center Freiburg	EPI_ISL_852739	Freiburg area	EPI_ISL_852659	Immunosuppressed patient (day 42)
EPI_ISL_852730	Freiburg area	EPI_ISL_852736	Freiburg area	EPI_ISL_852709	Immunosuppressed patient (day 0)
EPI_ISL_852780	Medical center Freiburg	EPI_ISL_852735	Freiburg area	EPI_ISL_852671	Immunosuppressed patient (day 7)
EPI_ISL_852777	Freiburg area	EPI_ISL_852768	Medical center Freiburg		
EPI_ISL_852776	Medical center Freiburg	EPI_ISL_852675	Medical center Freiburg		
EPI_ISL_852728	Medical center Freiburg	EPI_ISL_852674	Medical center Freiburg		
EPI_ISL_852726	Medical center Freiburg	EPI_ISL_852767	Medical center Freiburg		
EPI_ISL_852725	Freiburg area	EPI_ISL_852673	Freiburg area		
EPI_ISL_852724	Freiburg area	EPI_ISL_852672	Medical center Freiburg		
EPI_ISL_852722	Medical center Freiburg	EPI_ISL_852669	Freiburg area		
EPI_ISL_852721	Medical center Freiburg	EPI_ISL_852764	Freiburg area		

Extended Data Table 2: List of GISAID accession numbers of sequences from Freiburg. Sequence accession numbers of full-length SARS-CoV-2 genome sequences generated from swabs of patients at the University Medical Center, Freiburg, Germany between February and April and of the immunosuppressed patient.

Accession ID	Originating Laboratory	Submitting Laboratory	Authors
EPI_ISL_414508	Center of Medical Microbiology, Virology, and Hospital Hygiene, University of Duesseldorf	Center of Medical Microbiology, Virology, and Hospital Hygiene, University of Duesseldorf	Ortwin Adams, Marcel Andree, Alexander Dilthey, Torsten Feldt, Sandra Hauka, Torsten Houwaart, Björn-ErikJensen, Detlef Kindgen-Milles, Malte Kohns Vasconcelos, Klaus Pfeffer, Tina Senff, Daniel Strelow, JörgTimm, Andreas Walker, Tobias Wienemann
EPI_ISL_414521	Bundeswehr Institute of Microbiology	Bundeswehr Institute of Microbiology	Mathias C Walter, Markus H Antwerpen and Roman Wölfel
EPI_ISL_417458, EPI_ISL_417468, EPI_ISL_419552	Center of Medical Microbiology, Virology, and Hospital Hygiene, University of Duesseldorf	Center of Medical Microbiology, Virology, and Hospital Hygiene, University of Duesseldorf	Ortwin Adams, Marcel Andree, Alexander Dilthey, Torsten Feldt, Sandra Hauka, Torsten Houwaart, Björn-ErikJensen, Detlef Kindgen-Milles, Malte Kohns Vasconcelos, Klaus Pfeffer, Tina Senff, Daniel Strelow, JörgTimm, Andreas Walker, Tobias Wienemann
EPI_ISL_420899, EPI_ISL_420901, EPI_ISL_420902, EPI_ISL_420907, EPI_ISL_420912	Max von Pettenkofer Institute, Virology, National Reference Center for Retroviruses, LMU Munich	Laboratory for Functional Genome Analysis, Dept. Genomics, Gene Center of the LMU Munich	Max Muenchhoff, Stefan Krebs, Alexander Graf, Ashok Varadharajan, Oliver Keppler, Helmut Blum
EPI_ISL_425123, EPI_ISL_425125	Center of Medical Microbiology, Virology, and Hospital Hygiene, University of Duesseldorf	Center of Medical Microbiology, Virology, and Hospital Hygiene, University of Duesseldorf	Ortwin Adams, Marcel Andree, Alexander Dilthey, Torsten Feldt, Sandra Hauka, Torsten Houwaart, Björn-ErikJensen, Detlef Kindgen-Milles, Malte Kohns Vasconcelos, Klaus Pfeffer, Tina Senff, Daniel Strelow, JörgTimm, Andreas Walker, Tobias Wienemann
EPI_ISL_437215, EPI_ISL_437217, EPI_ISL_437221, EPI_ISL_437241, EPI_ISL_437245, EPI_ISL_437248, EPI_ISL_437249, EPI_ISL_437260, EPI_ISL_437266, EPI_ISL_437270, EPI_ISL_437271, EPI_ISL_437272, EPI_ISL_437274, EPI_ISL_437276, EPI_ISL_437278, EPI_ISL_437283, EPI_ISL_437287, EPI_ISL_437290, EPI_ISL_437292, EPI_ISL_437295, EPI_ISL_451944, EPI_ISL_466888, EPI_ISL_466892			
see above	Max von Pettenkofer Institute, Virology, National Reference Center for Retroviruses, LMU München	Laboratory for Functional Genome Analysis, Dept. Genomics, Gene Center of the LMU Munich	Max Muenchhoff, Stefan Krebs, Alexander Graf, Oliver Keppler, Helmut Blum
EPI_ISL_490205, EPI_ISL_490207	MünchenKlinik Schwabing	MGZ Medical Genetics Center	Dieter A. Wolf, Elke Holinski-Feder
EPI_ISL_513299, EPI_ISL_513300	Department of Infection Prevention and Infectious Diseases, University Hospital Regensburg	University Hospital Regensburg	Fritsch,J., Holzmann,T., Schneider-Brachert,W.
EPI_ISL_516630, EPI_ISL_516631, EPI_ISL_516632, EPI_ISL_516639, EPI_ISL_516640, EPI_ISL_516644	Charite Universitatsmedizin Berlin, Institut fur Virologie/Labor Berlin	Charite Universitatsmedizin Berlin, Institut fur Virologie/Labor Berlin	Victor M Corman, Barbara Muhlemann, JörnBeheim-Schwarzbach, Julia Schneider, Talitha Veith, Terry Jones, Christian Drosten
EPI_ISL_523934, EPI_ISL_523940, EPI_ISL_523945, EPI_ISL_523949	Center of Medical Microbiology, Virology, and Hospital Hygiene, University of Duesseldorf	Center of Medical Microbiology, Virology, and Hospital Hygiene, University of Duesseldorf	Maximilian Damagnez, Alexander Dilthey, Torsten Houwaart, Malte Kohns Vasconcelos, Marek Korencak, Jessica Nicolai, Klaus Pfeffer, Hendrik Streeck, Daniel Strelow, JörgTimm, Andreas Walker, Tobias Wienemann
EPI_ISL_525473	Institute of Clinical Microbiology and Hygiene, University Hospital Regensburg	Institute of Clinical Microbiology and Hygiene, University Hospital Regensburg	Hiergeist, A.
EPI_ISL_602282, EPI_ISL_602288, EPI_ISL_602293, EPI_ISL_602294	Evangelisches Klinikum Bethel, Institut für Laboratoriumsmedizin, Mikrobiologie und Hygiene	Bielefeld University	David Brandt, Tobias Busche, Markus Haak, JörnKalinowski, Levin-Joe Klages, Christiane Scherer, Alexander Sczyrba, Marina Simunovic, Svenja Vinke
EPI_ISL_602469, EPI_ISL_602470, EPI_ISL_602471, EPI_ISL_602474, EPI_ISL_602475, EPI_ISL_602476, EPI_ISL_602479, EPI_ISL_602482, EPI_ISL_602485, EPI_ISL_602488, EPI_ISL_602498, EPI_ISL_602504, EPI_ISL_602505, EPI_ISL_602506, EPI_ISL_602507, EPI_ISL_602519, EPI_ISL_602524, EPI_ISL_626217			
see above	Institute for Virology, University Hospital Essen	Center of Medical Microbiology, Virology, and Hospital Hygiene, University of Duesseldorf	Olympia E. Anastasiou, Ulf Dittmer, Maximilian Damagnez, Alexander Dilthey, Torsten Houwaart, Lisanna Hülse,Malte Kohns Vasconcelos, Nadine Lübke, Jessica Nicolai, Klaus Pfeffer, Daniel Strelow, JörgTimm, Andreas Walker, Tobias Wienemann
EPI_ISL_631300	MVZ DIAMEDIS Diagnostische Medizin Sennestadt GmbH	Bielefeld University	David Brandt, Tobias Busche, Markus Haak, JörnKalinowski, Levin-Joe Klages, Christiane Scherer, Alexander Sczyrba, Marina Simunovic, Svenja Vinke
EPI_ISL_640223, EPI_ISL_640226, EPI_ISL_640228, EPI_ISL_640236, EPI_ISL_640247, EPI_ISL_640252, EPI_ISL_640253, EPI_ISL_640261	MVZ Laborärzte Singen	MVZ Laborärzte Singen	Jonas Schmidt, Frithjof Blessing, Sandro Berghaus, Folker Wenzel
EPI_ISL_723077, EPI_ISL_723107, EPI_ISL_723114, EPI_ISL_723115	Institute of Medical Genetics and Applied Genomics	Institute of Medical Genetics and Applied Genomics	Caspar Gross, Tina Ganzenmüller, Siri Göpel, Michaela Pogoda, Daniela Bezdan, Michael Sonnabend, Angel Angelov, Nicolas Casadei, Stephan Ossowski, Thomas Iftner, Michael Bitzer
EPI_ISL_729477, EPI_ISL_729489, EPI_ISL_729491, EPI_ISL_729514	Charité Universitätsmedizin Berlin, Institut für Virologie/Labor Berlin	Charité Universitätsmedizin Berlin, Institut für Virologie	Victor M Corman, Barbara Mühlemann, JörnBeheim-Schwarzbach, Talitha Veith, Julia Schneider, Terry Jones, Christian Drosten
EPI_ISL_729516, EPI_ISL_729520, EPI_ISL_729524, EPI_ISL_729525	A. Krumbholz, Labor Dr. Krause und Kollegen MVZ GmbH, Kiel	Charité Universitätsmedizin Berlin, Institut für Virologie	Victor M Corman, Barbara Mühlemann, JörnBeheim-Schwarzbach, Talitha Veith, Julia Schneider, Terry Jones, Christian Drosten
EPI_ISL_729530	Charité Universitätsmedizin Berlin, Institut für Virologie/Labor Berlin	Charité Universitätsmedizin Berlin, Institut für Virologie	Victor M Corman, Barbara Mühlemann, JörnBeheim-Schwarzbach, Talitha Veith, Julia Schneider, Terry Jones, Christian Drosten
EPI_ISL_729536, EPI_ISL_729541, EPI_ISL_729546, EPI_ISL_729550	A. Krumbholz, Labor Dr. Krause und Kollegen MVZ GmbH, Kiel	Charité Universitätsmedizin Berlin, Institut für Virologie	Victor M Corman, Barbara Mühlemann, JörnBeheim-Schwarzbach, Talitha Veith, Julia Schneider, Terry Jones, Christian Drosten
EPI_ISL_732554, EPI_ISL_732555	Bundeswehr Institute of Microbiology	Bundeswehr Institute of Microbiology	Markus Antwerpen, Alexandra Rehn, Mathias Walter, Malena Bestehorn-Willmann, Sabine Zange, Enrico Georgi, Roman Wölfel
EPI_ISL_753798, EPI_ISL_753811, EPI_ISL_753924, EPI_ISL_753937, EPI_ISL_753942, EPI_ISL_754026, EPI_ISL_754028, EPI_ISL_754034, EPI_ISL_754041, EPI_ISL_754046, EPI_ISL_754050			
see above	Charité Universitätsmedizin Berlin, Institut für Virologie/Labor Berlin	Charité Universitätsmedizin Berlin, Institut für Virologie	Victor M Corman, JörnBeheim-Schwarzbach, Barbara Mühlemann, Julia Schneider, Talitha Veith, Terry Jones, Christian Drosten
EPI_ISL_763086	Jena University Hospital, Institute for Infectious Diseases and Infection Control	Institute of infectious medicine & hospital hygiene, CaSe-Group	Spott, Riccardo; Marquet, Mike; Pletz, Matthias W.; Brandt, Christian
EPI_ISL_775905, EPI_ISL_775911, EPI_ISL_775914, EPI_ISL_775918, EPI_ISL_775941, EPI_ISL_775944, EPI_ISL_775949, EPI_ISL_775958, EPI_ISL_775967, EPI_ISL_775968, EPI_ISL_775974, EPI_ISL_775977, EPI_ISL_775979, EPI_ISL_775983, EPI_ISL_775996, EPI_ISL_775998, EPI_ISL_776002, EPI_ISL_776017, EPI_ISL_776020, EPI_ISL_776035, EPI_ISL_776038, EPI_ISL_776040, EPI_ISL_776048, EPI_ISL_776061, EPI_ISL_776066, EPI_ISL_776070, EPI_ISL_776076, EPI_ISL_776079, EPI_ISL_776082, EPI_ISL_776087, EPI_ISL_776093, EPI_ISL_776094, EPI_ISL_776095, EPI_ISL_776100, EPI_ISL_776103, EPI_ISL_776105, EPI_ISL_776106, EPI_ISL_776108, EPI_ISL_776122, EPI_ISL_776123, EPI_ISL_776125, EPI_ISL_776127, EPI_ISL_776134, EPI_ISL_776140, EPI_ISL_776157, EPI_ISL_776160, EPI_ISL_776170, EPI_ISL_776172, EPI_ISL_776178, EPI_ISL_776191, EPI_ISL_776192, EPI_ISL_776193, EPI_ISL_776201, EPI_ISL_776214, EPI_ISL_776227, EPI_ISL_776230, EPI_ISL_776231, EPI_ISL_776237, EPI_ISL_776242, EPI_ISL_776246, EPI_ISL_776253, EPI_ISL_776254, EPI_ISL_776257, EPI_ISL_776258, EPI_ISL_776260, EPI_ISL_776261, EPI_ISL_776262, EPI_ISL_776266, EPI_ISL_776270, EPI_ISL_776275, EPI_ISL_776286, EPI_ISL_776292, EPI_ISL_776293, EPI_ISL_776295, EPI_ISL_776312, EPI_ISL_776313, EPI_ISL_776315, EPI_ISL_776317, EPI_ISL_776320, EPI_ISL_776322, EPI_ISL_776326, EPI_ISL_776340, EPI_ISL_776345, EPI_ISL_776355, EPI_ISL_776360, EPI_ISL_776395, EPI_ISL_776397, EPI_ISL_776410, EPI_ISL_776411, EPI_ISL_776424, EPI_ISL_776427, EPI_ISL_776434, EPI_ISL_776454, EPI_ISL_776473, EPI_ISL_776474, EPI_ISL_776478, EPI_ISL_776481, EPI_ISL_776491, EPI_ISL_776493, EPI_ISL_776501, EPI_ISL_776505, EPI_ISL_776507, EPI_ISL_776515, EPI_ISL_776557			
see above	University Medical Center Hamburg Eppendorf	Heinrich Pette Institute, Leibniz Institute for Experimental Virology	Alexis Robitaille, Thomas Günther, Johannes Knobloch, Martin Aepfelbacher, Nicole Fischer, Adam Grundhoff
EPI_ISL_806528, EPI_ISL_806530, EPI_ISL_806532, EPI_ISL_806533, EPI_ISL_806539	Charité Universitätsmedizin Berlin, Institut für Virologie/Labor Berlin	Charité Universitätsmedizin Berlin, Institut für Virologie	Victor M Corman, JörnBeheim-Schwarzbach, Barbara Mühlemann, Julia Schneider, Talitha Veith, Cornelia Schlee, Tomasz Zemojtel, Terry Jones, Christian Drosten
EPI_ISL_883163, EPI_ISL_883164, EPI_ISL_883167	Hannover Medical School, Institute of Virology	Hannover Medical School, Institute of Virology	Lars Steinbrück, Jasper Götting
EPI_ISL_883179, EPI_ISL_883182, EPI_ISL_883184, EPI_ISL_883188	UK Tübingen, Medical Microbiology	Hannover Medical School, Institute of Virology	Lars Steinbrück, Jasper Götting
EPI_ISL_887331, EPI_ISL_887335, EPI_ISL_887353, EPI_ISL_887354, EPI_ISL_887357, EPI_ISL_887360, EPI_ISL_887369, EPI_ISL_887370, EPI_ISL_887379, EPI_ISL_887386, EPI_ISL_887395, EPI_ISL_887397, EPI_ISL_887400, EPI_ISL_887403, EPI_ISL_887415			
see above	Protzer Lab	Protzer Lab, Gagneur Lab, Robert Koch Institut	Ulrike Protzer, Dieter Hoffmann, Eva Schulte, Andrea Theumer, Oliver Drechsel, Max von Kleist,Aleksandar Radonic,Stephan Fuchs, Alexander Karollus, Julien Gagneur
EPI_ISL_983571, EPI_ISL_983574, EPI_ISL_983578, EPI_ISL_983580, EPI_ISL_983581, EPI_ISL_983582, EPI_ISL_983587	Institute of Virology, University Hospital, University of Bonn and German Center for Infection Research (DZIF), Bonn-Cologne, Bonn, Germany	Institute of Virology, University Hospital, University of Bonn and German Center for Infection Research (DZIF), Bonn-Cologne, Bonn, Germany	Marek Korencak et al

Extended Data Table 3: Detailed list of GISAID accession numbers of the 250 randomly selected sequences from Germany between February and April 2020. We gratefully acknowledge the following authors from the originating laboratories responsible for obtaining the specimens, as well as the submitting laboratories where the genome data were generated and shared via GISAID, on which this research is based. All submitters of data may be contacted directly via www.gisaid.org. Authors are sorted alphabetically.